Vietnam Journal of Earth Sciences, 44(3), 301-326, https://doi.org/10.15625/2615-9783/16842

Vietnam Academy of Science and Technology
Vietnam Journal of Earth Sciences
http://www.vjs.ac.vn/index.php/jse

Geochemistry, zircon U-Pb geochronology and Sr-Nd-Hf isotopic composition of the Cha Val plutonic rocks in central Vietnam: Implications for Permian-Triassic Paleo-Tethys subduction-related magmatism

Phạm Minh[1,2], Pham Trung Hieu[1,2*], Kenta Kawaguchi[3,4], Anh Thi Quynh Nong [1,2], Le Duc Phuc[1,2]

[1]*Faculty of Geology, University of Science, Ho Chi Minh City, Vietnam*
[2]*Vietnam National University, Ho Chi Minh City, Vietnam*
[3]*Department of Earth and Environmental Sciences, Jeonbuk National University, Jeonju, Republic of Korea*
[4]*Department of Earth and Planetary Systems Science, Graduate School of Science, Hiroshima University, Higashi-Hiroshima, Japan*

Received 07 October 2021; Received in revised form 05 November 2021; Accepted 20 December 2021

ABSTRACT

The Cha Val plutonic rocks emplaced in the south of the Truong Son belt (north of Kontum massif, Central Vietnam) together with abundant Permian-Triassic magmatic rocks. This magmatic complex provides important information to reconstruct the tectonic evolution of the Indochina block and surrounding areas. The Cha Val plutonic rocks mainly comprise diorite, quartz diorite, and granodiorite. Geochemically, they are metaluminous with low A/CNK (0.49 to 1.16 with an average of 0.85), medium to high K, low to medium SiO_2, and $Na_2O/K_2O>1$. Trace and rare earth element compositions display enrichment in Cs, U, Pb, and Nd, but depletion in Ba, Nb, Ta, P, Eu, and Ti, similar to those of continental arc-related magmas. Rock-forming minerals of the Cha Val plutonic rocks are characterized by abundant hornblende. All observed petrographical and geochemical characteristics suggest that the Cha Val plutonic rocks are typical for I-type affinity generated from a subduction regime. LA-ICP-MS U-Pb zircon analyses of three representative samples yielded their crystallization ages between 258.0 Ma and 248.9 Ma, temporally coeval with Late Permian-Early Triassic magmatism previously reported in the Truong Son belt. The $(^{87}Sr/^{86}Sr)_i$ ratios (0.7081 to 0.7244), negative whole-rock $\varepsilon_{Nd}(t)$ values (-4.5 to -2.9), zircon $\varepsilon_{Hf}(t)$ values (-1.04 to 2.71), and whole-rock Nd and zircon Hf model ages (T_{DM2}) (1394 Ma to 1111 Ma) indicate that the Cha Val plutonic rocks are derived from melting of Mesoproterozoic crustal materials with a minor contribution of mantle-derived melt. Together with other Permian-Triassic magmatic complexes along the Song Ma suture zone and the Truong Son Belt, the Cha Val plutonic rocks are a representative of magmatism associated with the subduction-collision that amalgamated the South China and Indochina blocks after the closure of a branch of Paleo-Tethys along the Song Ma suture zone during the Late Permian-Early Triassic Indosinian orogeny.

Keywords: Geochemistry, zircon U-Pb geochronology, Sr-Nd-Hf isotopic composition, Cha Val complex, Truong Son belt, oceanic subduction, Indosinian orogeny.

1. Introduction

Southeast Asia was formed by amalgamating several continental blocks, such as South China, Indochina, Sibumasu, and Simao blocks, which were rifted from the northern Gondwana supercontinent (Tri and

*Corresponding author, Email: pthieu@hcmus.edu.vn

Khuc, 2011; Metcalfe, 2013; Thanh et al., 2019). Permian-Triassic magmatic activities are widespread along the Song Ma suture. The Truong Son belt (Fig.1a) and are widely considered to result from the closure of Paleo-Tethys ocean leading to the South China-Indochina collision (Shi et al., 2015; Ngo et al., 2016; Hieu et al., 2017; Thanh et al., 2019; Qian et al., 2019). They are meaningful information to constrain the regional magmatic-tectonic evolutionary history of the Indochina block and surrounding areas. Recent studies suggest that the Song Ma suture is the plate boundary between the South China and Indochina blocks which amalgamated during the Permian-Triassic (Lepvrier et al., 2008; Faure et al., 2014; Hieu et al., 2017; Thanh et al., 2019). Magmatic rocks in the northern Truong Son belt have been well studied (e.g., Lepvrier et al., 2008; Faure et al., 2014; Shi et al., 2015; Ngo et al., 2016; Hieu et al., 2017; Thanh et al., 2019; Qian et al., 2019), however, the southern part of the Truong Son belt is still unclear.

The Cha Val plutonic rocks include small-sized intrusions have identified by geological mapping and mineral prospecting at scale 1:200 000 of the Hue-Quang Ngai sheet (Trang et al., 1984; Faure et al., 2014) and are an essential constituent of the southern Truong Son belt. According to Trang et al. (1984), the Cha Val formation was described as an independent complex (Cha Val complex) mainly comprising gabbronorite, gabbro-pyroxenite, and gabbro-diorite. However, Tri and Khuc (2011) classified the Cha Val complex as a series of minor mafic-ultramafic intrusions as the Phu Loc complex with the main petrographic composition gabbro-pyroxenite. Later, in the report on geological mapping and mineral investigation of the A Hoi - Phuoc Hao sheet at scale 1:50.000 (Vinh, 2012), the Cha Val plutonic rocks were merged into Permian Ben Giang-Que Son complex with more felsic-dominant compositions of diorite and quartz diorite. Regarding the formation mechanism of the Cha Val plutonic rocks, there have been different views: (1) Tri and Khuc (2011) proposed that they were formed due to arc magmatism associated with subduction (active continental margin), (2) Owada et al. (2007); Tran et al. (2020) suggested that Late Permian-Early Triassic magmatic formations were related to the Emeishan mantle plume. The detailed investigations on the Cha Val plutonic rocks have documented the magmatic emplacement ages acquired mainly by the K-Ar method (Tri and Khuc, 2011). Only one gabbroic sample was dated using the LA-ICP-MS U-Pb zircon method (Tran et al., 2020). Despite these scattered dating results, the geochemical characteristics, isotopic composition, and petrogenesis of the Cha Val plutonic rocks have not received adequate attention.

This study presents new data on the geochemical characteristics, U-Pb geochronology, and Sr-Nd-Hf isotopic compositions of the Cha Val plutonic rocks to clarify their origin and tectonic setting in the study area, contributing to deciphering the regional magmatic evolutionary history of Indochina during the Permian-Triassic.

2. Geological setting and petrography

On the territory of Vietnam, according to the viewpoints of Vietnamese and foreign geologists, the Indochina block is divided into three major structural zones: the Da Lat zone in the south, the Kontum massif in the center, and the Truong Son belt in the north (e.g., Lepvrier et al., 2004; Hoa et al., 2008; Tri and Khuc, 2011; Hieu et al., 2015; Kawaguchi et al., 2021) (Fig. 1a). The northern boundary of the Truong Son belt (north-central Vietnam) is the Song Ma suture (Metcalfe, 1999; 2013; Thanh et al., 2011; Zhang et al., 2013; Faure

et al., 2014; Hieu et al., 2017; Thanh et al., 2019). To the south, the Truong Son belt is bordered by the Tam Ky - Phuoc Son suture, which is also considered a boundary separating the Truong Son area (Truong Son terrane) from the Kontum massif (Tran et al., 2014; Nguyen et al., 2019).

The Truong Son belt (Fig. 1a), which is located between the Song Ma suture and Kontum massif, consists of prevalent northwest-southeast left-lateral faults, such as Khe Sanh-Da Nang fault and Song Ca fault, identical with the orientation of the Song Ma suture (Lepvrier et al., 1997). Stratigraphically, the Truong Son belt exposes ancient formations such as Neoproterozoic quartz schist and Cambro-Ordovician quartz-sericite schist, Permian-Triassic plutonic-volcanic magmatic bodies, Triassic and Jurassic conglomerate, sandstone, and siltstone (Fig. 1b). Plutonic and volcanic complexes have petrogenesis with ages ranging from Permian to Triassic such as the Dien Bien, Song Ma, Phia Bioc, Truong Son, Hai Van, Chal Val, and Ben Giang-Que Son complexes and Dong Trau formation and they build up the main part of the Truong Son belt. The Permian-Triassic plutonic and volcanic complexes along the Truong Son belt and the Song Ma suture zone are attributed to different tectonic settings corresponding to three phases of the accretion between the South China and Indochina blocks: subduction (290-250 Ma), syn-collision (250-240 Ma), and post-collision (240-210 Ma) (Hoa et al., 2008; Liu et al., 2012; Nakano et al., 2013; Hieu et al., 2015; 2017; 2019; Thanh et al., 2019). The subduction phase generated numerous I-type granites (Dien Bien granite, Chieng Khuong granite, Song Ma granite, and Cha Val plutonic rocks; Liu et al., 2012; Hieu et al., 2017 and this study) (Fig. 10b), while the syn-collision phase developed abundant S-type granites (Muong Lat granite, Phia Bioc granite, and Hai Van granite; Hieu et al., 2015; Thanh et al., 2019). In the final phase, the post-collisional setting again emplaced sporadic I-type granites (Muong Luan granite; Hieu et al., 2019).

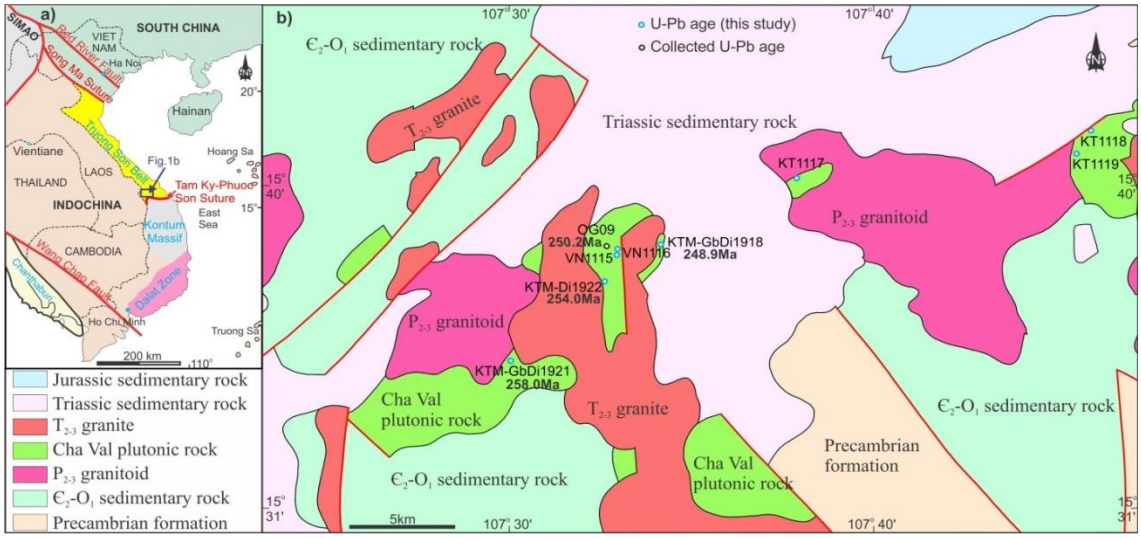

Figure 1. (a) Geological tectonic framework of Southeast Asia, showing three major structural zones in the Indochina block (Tri and Khuc, 2011). (b) Simplified geological map of the study area in the southern part of Truong Son belt (modified after Trang, 1994). The geochronological data is compiled from Tran et al. (2020) and obtained in this study

The Cha Val plutonic rocks distributed in the west of Hoi An city, Quang Nam province, include some elliptical bodies (Fig. 2a) with an exposed area of about 79 km^2 and are penetrated by the Hai Van granites. This study collected eleven samples from the Cha Val plutons in Quang Nam province along National Highway 14D, cutting through the Cha Val bodies. Sampling coordinates and localities are shown in Fig. 1b and Table 1. In the field, the Cha Val plutonic bodies are weathered on the surface and are covered by eluvial sediments with a thickness of 0.5 to 1m. The main petrographical components of the Cha Val plutonic rocks are dark-gray hornblende-rich diorite, quartz diorite, and granodiorite (Fig. 2b). The Cha Val plutonic rocks show a massive structure and an equigranular and euhedral to the subhedral texture of major rock-forming minerals (plagioclase and hornblende are more euhedral than other minerals), and a fine- to medium-grained size. Mineral compositions comprise plagioclase (40-45%), hornblende (20-35%), quartz (0-15%), biotite (0-15%), and K-feldspar (0-5%) (Figs. 2c-h). The common accessory minerals are zircon, apatite, titanate, and metallic oxides. Observations under optical microscopes show oscillatory zonation of plagioclases, albite twinning characteristic for andesine, and prevalent sericitization. Hornblende exhibits little alteration and is strongly pleochroic. Quartz is commonly subhedral in shape. Biotite is brown, strongly polychromatic, and partly chloridized.

Table 1. Major element contents and CIPW of the Cha Val plutonic rocks

Sample	V1115	V1116-1	V1116-2	V1116-3	V1117	V1118	V1118P	V1119	KTM-GbDi1918	KTM-GbDi1921	KTM-Di1922
Lithology	granodiorite	quartz diorite	micro-granodiorite	diorite	quartz diorite	diorite	diorite	quartz diorite	diorite	quartz diorite	diorite
Latitude	15°38'05.2"N	15°38'14.1"N	15°38'14.1"N	15°38'14.1"N	15°40'22.4"N	15°41'49.1"N	15°41'49.1"N	15°41'30.5"N	15°38'26.1"N	15°35'16.5"N	15°37'42.7"N
Longtitude	107°32'58.5"E	107°33'06.4"E	107°33'06.4"E	107°33'06.4"E	107°38'08.0"E	107°46'12.5"E	107°46'12.5"E	107°46'07.4"E	107°34'11.5"E	107°30'06.3"E	107°32'35.0"E
SiO_2	66.39	55.63	67.93	52.20	60.11	51.88	51.98	55.13	53.43	58.58	56.83
TiO_2	0.59	0.70	0.38	0.94	0.65	0.99	0.99	0.91	1.36	1.12	0.49
Al_2O_3	16.16	10.91	12.93	16.37	17.47	18.17	18.16	16.89	18.63	16.80	18.89
$Fe_2O_3^t$	4.69	7.71	6.51	8.91	5.63	8.30	8.34	8.48	7.88	7.22	5.98
MnO	0.08	0.14	0.36	0.14	0.10	0.15	0.15	0.14	0.11	0.13	0.10
MgO	1.33	9.74	1.62	5.82	2.47	4.70	4.71	4.08	3.62	3.61	4.04
CaO	2.71	9.34	5.95	8.81	6.05	7.72	7.73	5.59	7.38	6.25	7.18
Na_2O	3.92	2.29	1.83	2.86	4.09	3.73	3.74	4.33	3.81	3.34	4.01
K_2O	2.40	1.34	1.16	1.54	1.54	1.74	1.75	1.89	1.89	1.54	1.24
P_2O_5	0.19	0.20	0.08	0.29	0.22	0.31	0.31	0.20	0.46	0.34	0.24
LOI	2.02	0.94	0.78	1.40	1.20	1.72	1.66	2.28	0.88	1.30	4.88
Total	100.48	98.93	99.53	99.27	99.53	99.40	99.51	99.92	98.57	98.93	98.98
Fe*	0.76	0.42	0.78	0.58	0.67	0.61	0.61	0.65	0.66	0.64	0.57
Mg#	35.96	71.44	33.01	56.40	46.49	52.86	52.80	48.79	47.66	49.75	57.21
A/CNK	1.16	0.49	0.86	0.73	0.90	0.82	0.82	0.87	0.86	0.91	0.90
A/NK	1.79	2.09	3.03	2.57	2.08	2.26	2.26	1.84	2.24	2.35	2.38
Q	24.56	4.57	34.82	0.30	11.81			0.90	0.59	11.66	5.03
C	2.68										
Or	14.40	8.08	6.94	9.30	9.25	10.53	10.57	11.44	11.33	9.18	7.41
Ab	33.69	19.78	15.68	24.73	35.19	32.31	32.34	37.52	32.72	28.58	34.24
An	12.39	15.84	23.95	27.87	25.18	28.34	28.19	21.59	28.54	26.59	30.20
Di(FS)		6.99	3.19	5.30	1.71	3.38	3.44	2.32	2.30	1.02	1.49
Di(MS)		17.34	1.44	6.94	1.52	3.89	3.95	2.24	2.30	1.08	1.97
Hy(MS)	3.37	16.72	3.42	11.59	5.55	5.11	5.04	9.37	8.09	8.59	9.24
Hy(FS)	6.64	7.72	8.70	10.15	7.17	5.09	5.04	11.12	9.27	9.30	8.05
Ol(MS)						3.56	3.59				
Ol(FS)						3.91	3.95				
Mt	0.69	1.14	0.96	1.32	0.83	1.23	1.24	1.26	1.16	1.06	0.88
Il	1.14	1.36	0.73	1.82	1.26	1.92	1.92	1.77	2.61	2.14	0.94
Ap	0.45	0.47	0.19	0.69	0.52	0.73	0.73	0.48	1.08	0.79	0.56

A/CNK value: molar $Al_2O_3/(CaO + Na_2O + K_2O)$; A/NK value: molar $Al_2O_3/(Na_2O + K_2O)$

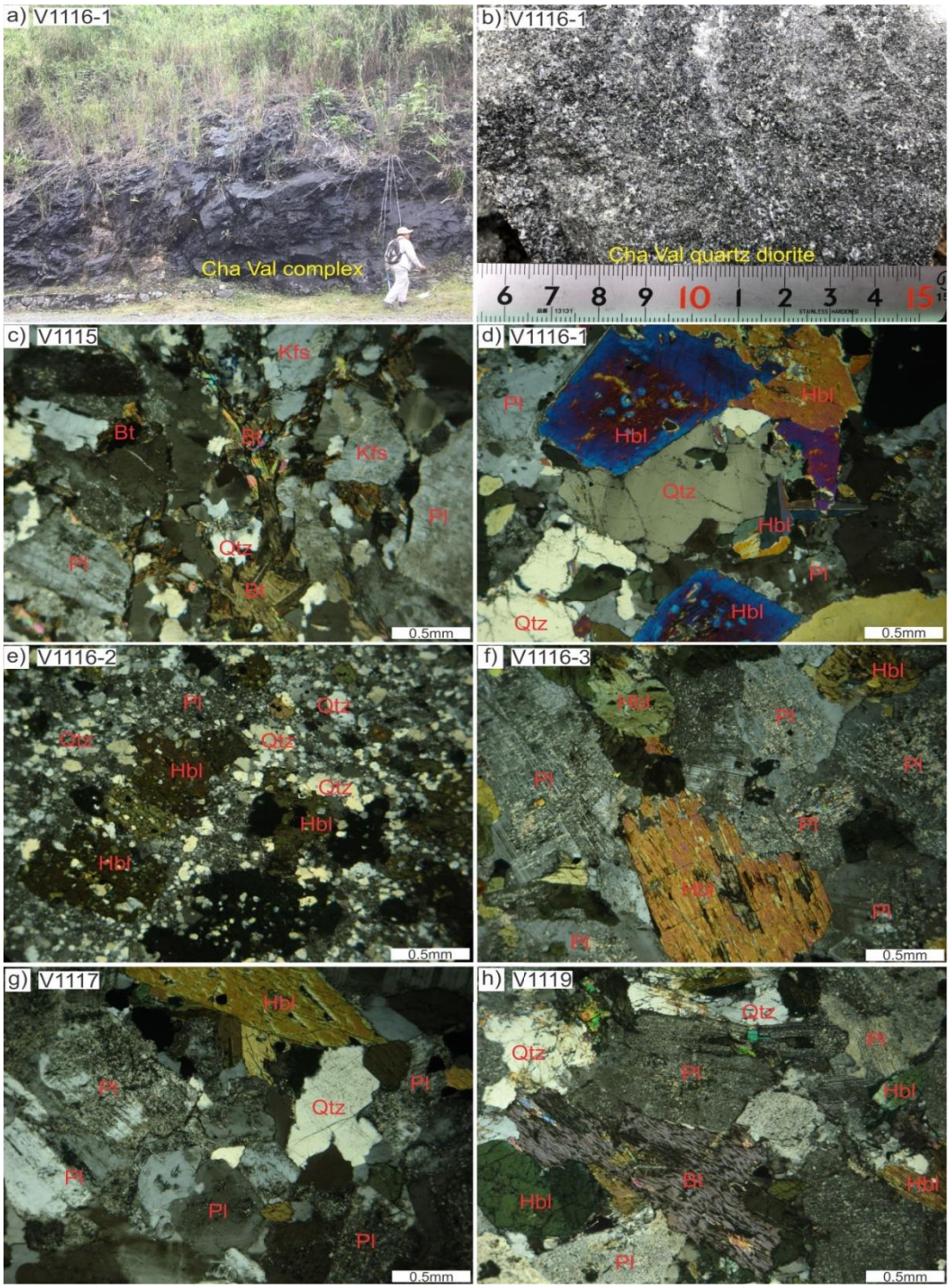

Figure 2. Outcrop features and thin-section photographs of the Cha Val plutonic rocks: (a) Cha Val pluton, GPS: 15°38'14.1"N, 107°33'06.4"E; (b) Cha Val medium-grained diorite, GPS: 15°38'14.1"N, 107°33'06.4"E; and (c)-(h) Cross-polarized light photomicrographs of Cha Val minerals. Mineral abbreviations: Pl: plagioclase, Hbl: Hornblende, Bt: biotite, Qtz: quartz, K-feldspar: Kfs

3. Analytical methods

Selected samples of the Cha Val complex were prepared and processed to obtain whole-rock geochemical compositions. Analyses were conducted at two places: the Institute of Geology and Geophysics, Chinese Academy of Sciences, Beijing, China (eight samples: V1115, V1116-1, V1116-2. V1116-3, V1117, V1118, V1118P, and V1119) and the Department of Earth and Planetary Systems Science, Hiroshima University, Japan (three samples: KTM-GbDi1918, KTM-GbDi1921, and KTM-Di1922).

Eight samples analyzed in China were crushed and then powdered to less than 200 mesh grain size. X-ray fluorescence spectrometry (XRF) was used to obtain significant element compositions using the standard sample GBW07103 for external control of analytical quality. For trace and rare earth elements, an Agilent 7500a inductively coupled plasma mass spectrometry was applied, and the standard BHVO-2 was used to monitor the analytical quality. Uncertainties were reported at less than 5% for major and trace element compositions. The detailed procedures of measurement follow Peng et al. (2012). The analytical results are presented in Tables 1 and 2.

Three samples analyzed in Japan were eliminated altered parts, crushed, and then powdered with an agate ball vibration mill. The fine powder was ignited at 950°C for six hours to determine loss on ignition (LOI). Major element analyses were carried out using X-ray fluorescence spectrometry (XRF: Rigaku ZSX-101e). X-rays produced by a 3 kW Rh/W dual anode tube were radiated on fused bead samples. The analytical precision (1σ) of major elements measured in XRF is less than 0.14 wt.%, and that of trace elements ranges between 0.44 (Yb) to 2.46 (Sr) and 8.55 (Ba) ppm (Kawaguchi et al., 2020).

Standard density and magnetic techniques separated zircon grains from the Cha Val plutonic rocks. Representative zircon grains with few fractures were handpicked under a binocular microscope. Selected zircons were mounted in an epoxy resin disk together with the zircon consistency standard YO1 (TIMS 206Pb/238U age of 279.3 Ma; Herzig et al., 1997). They were polished to expose the cores of zircon grains. To study their morphology and internal structures and determine spot positions for U-Pb dating measurements, all zircons were analyzed under transmitted and reflected light and cathodoluminescence (CL) images obtained from a scanning electron microscope (SEM: JEOL JSM 7500F). A laser spot size was maintained at 25 μm and the repetition rate at 4Hz. The analyses were carried out at the Department of Earth and Planetary Systems Science, Hiroshima University, Japan. The weighted mean ages were obtained at a 95% confidence level, and the ages and isotopic ratios were analyzed at a 2σ confidence level. Data reduction was carried out using the program Pepi-AGE (Dunkl et al., 2008) and the final statistical plotting using Isoplot/Ex (Ludwig, 2003). The detailed procedures were described by Kawaguchi et al. (2020).

A Thermo Finnigan Neptune multi-collector ICP-MS and a Geolas CQ 193 nm laser ablation system based at the Institute of Geology and Geophysics, Chinese Academy of Sciences, Beijing were used to perform *in situ* Lu-Hf isotopic measurements. The pulse rate was maintained at 10 Hz and the beam diameter at 44 μm. Standard zircon 91500 was analyzed as an external standard. Analytical procedures and interference correction method of ^{176}Yb on ^{176}Hf are similar to those reported by Chu et al. (2002). The ^{176}Lu decay constant of 1.865×10^{-11}year^{-1} was adopted to calculate initial ^{176}Hf/^{177}Hf ratios (Scherer et al., 2001). The calculation of the ε_{Hf} values was based on the reported chondritic values of ^{176}Lu/^{177}Hf = 0.0336 and ^{176}Hf/^{177}Hf = 0.282785 (Blichert-Toft and Albarède, 1997). According to the

average continental crust (Griffin et al., 2002), the two-stage Hf model age (T_{DM2}) was calculated using $^{176}Lu/^{177}Hf$ = 0.015. The analytical results are shown in Table 4.

Table 2. Trace and rare earth element compositions of the Cha Val plutonic rocks

Sample	V1115	V1116-1	V1116-2	V1116-3	V1117	V1118	V1119	KTM-GbDi1918	KTM-GbDi1921	KTM-Di1922
Sc	8.88	10.8	5.97	15.3	13.4	19.9	17.8	16.28	16.08	13.42
V	5.11	413	1.2	40.7	15	31.7	12.4	156.72	125.56	71.35
Cr	4.98	370	1.71	36.9	13.1	28	11.2	17.67	57.51	23.64
Co	0.8	63.9	2.77	11.6	3.82	8.84	2.59	20.49	20.90	20.11
Ni	4.41	166	12.7	38.1	15.4	32.8	14.4	15.58	20.56	17.03
Cu	40	49.2	35.3	50	46.5	46.7	37.5	32.90	36.72	17.51
Zn	90.3	66.5	33.7	73.1	58.7	42.6	19.5	89.93	96.60	74.91
Ga	20.3	13.7	14.6	17.9	22.4	23.4	21.2	20.92	17.15	19.24
Rb	107	38.4	63.2	42.2	39.3	65.9	78.2	60.56	63.44	53.37
Sr	299	290	68	522	591	611	519	726.47	480.57	502.79
Zr	275	97.2	49.2	126	138	99	138	274.89	233.15	216.37
Nb	13.1	9.05	0.7	10.5	8.18	9.01	9.16	17.03	17.23	10.91
Cs	8.26	1.69	2.98	4.64	1.03	3.29	3.89	4.81	4.42	6.95
Ba	797	235	99.1	374	638	553	619	759.91	406.11	276.00
Hf	7.19	2.75	1.52	3.2	3.65	2.94	4.03	10.16	7.65	8.24
Ta	1.36	0.47	0.05	0.69	0.44	0.57	0.54			
Pb	18.6	7	12.6	6.96	7.29	4.2	3.54	6.81	10.60	10.20
Th	13.9	8.13	0.66	7.82	6.53	7.35	10.5	4.53	8.16	6.21
U	10.7	2.17	0.36	1.32	1.59	1.95	3.06	0.58	3.42	1.30
La	46	26	2.4	31.6	25.5	24.8	21.3	47.39	38.83	26.66
Ce	91.39	54.34	5.7855	65.455	46.4	55.6	45.6	91.96	71.73	52.48
Pr	9.17	5.86	0.76	6.81	5.16	6.85	5.57			
Nd	33.1	23	3.84	25.5	20	28.3	23	39.34	31.53	23.90
Sm	6.29	4.77	1.52	4.78	3.65	5.65	4.84			
Eu	1.24	1.13	0.55	1.36	1.04	1.48	1.31			
Gd	5.91	4.59	2.1	4.49	3.06	4.77	4.39			
Tb	0.84	0.65	0.4	0.62	0.41	0.66	0.65			
Dy	4.85	3.76	2.7	3.55	2.23	3.66	3.83			
Ho	0.97	0.77	0.65	0.73	0.43	0.72	0.77			
Er	2.53	2.03	1.89	1.95	1.19	2.01	2.18			
Tm	0.37	0.3	0.31	0.29	0.18	0.3	0.34			
Yb	2.57	2.03	2.26	1.97	1.23	2.06	2.32	3.37	1.94	0.86
Lu	0.38	0.3	0.36	0.3	0.2	0.32	0.37			
Y	27.7	22.3	19.8	21.4	12.6	20.9	22.7	28.56	27.74	19.42
Li	24.8	6.38	7.22	11.9	10.3	25.2	34.5			
Be	3.18	0.92	0.39	1.13	1.37	1.3	1.09			
T_{Zr} (°C)	838.00	600.31	671.22	678.42	735.21	678.30	719.97	766.75	776.03	761.74
10000Ga/Al	2.37	2.37	2.13	2.07	2.42	2.43	2.37	2.12	1.93	1.92
Eu/Eu*	0.62	0.74	0.94	0.90	0.95	0.87	0.87			
∑LREE	187.19	115.10	14.86	135.51	101.75	122.68	101.62	178.69	142.09	103.04
∑HREE	18.42	14.43	10.67	13.90	8.93	14.50	14.85	3.37	1.94	0.86
∑REE	205.61	129.53	25.53	149.41	110.68	137.18	116.47	182.06	144.03	103.90
(La/Yb)n	12.84	9.19	0.76	11.51	14.87	8.64	6.59	10.09	14.36	22.24
(Tb/Yb)n	1.49	1.46	0.80	1.43	1.52	1.46	1.27	0.00	0.00	0.00
(La/Nd)n	2.74	2.23	1.23	2.44	2.51	1.73	1.82	2.37	2.43	2.20
Ybn	15.12	11.94	13.29	11.59	7.24	12.12	13.65	19.82	11.41	5.06

T_{Zr} (°C) = 12,900/(2.95+0.85x((Na+K+2xCa)/(AlxSi))+ln$D^{Zr,zircon/melt}$) (Watson and Harrison, 1983); Eu/Eu* : $Eu_N/(Sm_N*Gd_N)^{1/2}$

Table 3. Zircon U-Pb analytical data of the Cha Val plutonic rocks

Spot Label	$^{238}U/^{206}Pb^{*} \pm 2\sigma$			$^{207}Pb^{*}/^{206}Pb^{*} \pm 2\sigma$			$^{206}Pb^{*}/^{238}U$ age (Ma, $\pm 2\sigma$)			$^{207}Pb^{*}/^{235}U$ age (Ma, $\pm 2\sigma$)			$^{207}Pb^{*}/^{206}Pb^{*}$ age (Ma, $\pm 2\sigma$)			Th/U Conc.%	
KTM-GbDi1918																	
73KTM1918	26.110	±	1.175	0.0551	±	0.0063	242.3	±	10.7	259.2	±	28.5	415.5	±	277.2	0.33	93
74KTM1918	25.119	±	0.929	0.0503	±	0.0039	251.7	±	9.1	247.7	±	19.1	210.4	±	191.6	0.24	102
75KTM1918	25.202	±	0.680	0.0523	±	0.0021	250.9	±	6.6	255.4	±	10.9	297.7	±	94.0	0.97	98
76KTM1918	25.510	±	1.071	0.0566	±	0.0057	247.9	±	10.2	271.2	±	26.0	477.7	±	237.8	0.42	91
77KTM1918	24.600	±	0.713	0.0509	±	0.0020	256.9	±	7.3	254.6	±	11.1	233.9	±	95.0	1.09	101
78KTM1918	25.297	±	0.885	0.0462	±	0.0056	249.9	±	8.6	228.1	±	26.1	8.2	±	8.1	0.47	110
79KTM1918	25.913	±	0.907	0.0521	±	0.0028	244.1	±	8.4	248.5	±	14.2	290.4	±	128.3	0.80	98
83KTM1918	25.536	±	0.689	0.0516	±	0.0018	247.7	±	6.6	249.5	±	9.8	266.7	±	82.3	0.77	99
84KTM1918	25.661	±	1.026	0.0551	±	0.0055	246.4	±	9.7	263.2	±	25.4	415.1	±	240.5	0.37	94
85KTM1918	22.573	±	0.926	0.0532	±	0.0026	279.4	±	11.2	285.5	±	16.1	335.7	±	115.0	0.85	98
86KTM1918	25.562	±	0.792	0.0526	±	0.0042	247.3	±	7.5	253.6	±	19.3	312.0	±	190.5	0.67	98
87KTM1918	24.331	±	0.827	0.0586	±	0.0039	259.7	±	8.7	291.3	±	18.9	553.7	±	150.9	0.23	89
88KTM1918	25.419	±	0.712	0.0514	±	0.0020	248.7	±	6.8	249.6	±	10.7	257.9	±	92.2	0.87	100
89KTM1918	25.820	±	1.239	0.0588	±	0.0064	244.9	±	11.5	277.3	±	29.3	560.3	±	257.2	0.36	88
93KTM1918	24.969	±	0.724	0.0509	±	0.0018	253.1	±	7.2	251.6	±	10.1	237.7	±	82.7	1.31	101
94KTM1918	25.050	±	0.852	0.0528	±	0.0037	252.3	±	8.4	258.9	±	18.2	318.8	±	170.0	0.73	97
95KTM1918	25.536	±	0.792	0.0524	±	0.0026	247.6	±	7.5	253.1	±	13.3	304.0	±	118.1	0.63	98
96KTM1918	25.634	±	0.846	0.0513	±	0.0027	246.7	±	8.0	247.3	±	13.7	252.8	±	124.2	1.10	100
97KTM1918	26.178	±	0.916	0.0511	±	0.0047	241.6	±	8.3	242.0	±	21.3	245.6	±	227.0	0.46	100
98KTM1918	25.272	±	0.783	0.0524	±	0.0024	250.2	±	7.6	255.4	±	12.5	303.8	±	108.4	0.88	98
KTM-GbDi1921																	
40KTM1921	25.291	±	1.138	0.0509	±	0.0051	250.0	±	11.0	248.6	±	24.8	235.9	±	235.8	0.37	101
41KTM1921	24.474	±	1.003	0.0489	±	0.0052	258.2	±	10.4	247.1	±	25.3	142.9	±	142.8	0.35	104
42KTM1921	23.946	±	0.862	0.0496	±	0.0032	263.7	±	9.3	255.0	±	16.8	176.0	±	159.1	0.51	103
43KTM1921	24.414	±	0.830	0.0504	±	0.0021	258.8	±	8.6	254.3	±	12.2	213.4	±	100.3	1.12	102
44KTM1921	25.132	±	0.955	0.0505	±	0.0050	251.6	±	9.4	248.5	±	23.6	219.7	±	219.6	0.41	101
45KTM1921	23.969	±	0.767	0.0508	±	0.0020	263.5	±	8.3	260.3	±	11.8	231.4	±	95.1	1.12	101
46KTM1921	24.661	±	0.962	0.0515	±	0.0034	256.2	±	9.8	257.0	±	17.6	264.5	±	159.0	0.54	100
50KTM1921	24.062	±	0.746	0.0501	±	0.0023	262.5	±	8.0	256.2	±	12.5	199.2	±	110.4	1.27	102
51KTM1921	23.781	±	0.618	0.0512	±	0.0016	265.5	±	6.8	264.0	±	9.3	250.7	±	73.0	1.15	101
52KTM1921	24.765	±	0.966	0.0512	±	0.0051	255.2	±	9.8	254.7	±	24.4	251.0	±	248.0	0.35	100
53KTM1921	24.777	±	0.867	0.0533	±	0.0044	255.1	±	8.8	263.5	±	21.1	339.6	±	199.8	0.52	97
54KTM1921	24.219	±	0.751	0.0514	±	0.0021	260.8	±	7.9	260.6	±	11.8	258.7	±	97.1	0.84	100
55KTM1921	23.872	±	0.716	0.0536	±	0.0027	264.6	±	7.8	273.8	±	14.3	353.3	±	119.6	0.54	97
56KTM1921	25.126	±	1.055	0.0499	±	0.0062	251.6	±	10.4	245.9	±	29.0	191.6	±	191.5	0.32	102
60KTM1921	24.851	±	0.820	0.0508	±	0.0020	254.3	±	8.2	252.1	±	11.7	231.5	±	95.1	1.18	101
61KTM1921	24.759	±	0.768	0.0539	±	0.0026	255.3	±	7.8	266.6	±	13.7	367.5	±	114.3	0.86	96
62KTM1921	23.127	±	1.041	0.0493	±	0.0049	272.9	±	12.0	261.7	±	25.5	162.2	±	162.1	0.57	104
63KTM1921	24.869	±	1.045	0.0523	±	0.0043	254.1	±	10.5	258.4	±	21.2	297.9	±	198.8	0.34	98
64KTM1921	24.894	±	0.971	0.0509	±	0.0023	253.9	±	9.7	252.3	±	13.5	238.0	±	109.7	0.82	101
65KTM1921	26.546	±	1.354	0.0565	±	0.0072	238.4	±	11.9	261.3	±	32.3	472.0	±	311.5	0.36	91
66KTM1921	25.773	±	0.851	0.0514	±	0.0017	245.4	±	8.0	246.8	±	10.3	259.8	±	77.7	1.08	99
KTM-Di1922																	
07KTM1922	24.438	±	0.733	0.0513	±	0.0019	258.5	±	7.6	258.0	±	11.0	253.4	±	87.4	1.27	100
08KTM1922	25.157	±	0.755	0.0499	±	0.0020	251.3	±	7.4	245.3	±	11.2	188.4	±	98.3	0.97	102
09KTM1922	24.195	±	0.653	0.0508	±	0.0015	261.1	±	6.9	258.0	±	9.2	230.4	±	70.8	0.60	101
10KTM1922	25.349	±	0.760	0.0510	±	0.0022	249.4	±	7.3	248.5	±	11.5	239.8	±	102.2	1.14	100
11KTM1922	25.006	±	0.750	0.0517	±	0.0019	252.8	±	7.4	254.7	±	10.9	272.3	±	87.1	0.86	99
12KTM1922	25.157	±	0.730	0.0532	±	0.0023	251.3	±	7.2	259.7	±	12.2	336.2	±	102.9	1.04	97
13KTM1922	24.343	±	0.657	0.0654	±	0.0022	259.5	±	6.9	319.9	±	11.9	786.9	±	70.8	0.76	81

Spot Label	$^{238}U/^{206}Pb^{*} \pm 2\sigma$			$^{207}Pb^{*}/^{206}Pb^{*} \pm 2\sigma$			$^{206}Pb^{*}/^{238}U$ age (Ma, ± 2σ)			$^{207}Pb^{*}/^{235}U$ age (Ma, ± 2σ)			$^{207}Pb^{*}/^{206}Pb^{*}$ age (Ma, ± 2σ)			Th/U Conc.%	
17KTM1922	24.468	±	0.734	0.0529	±	0.0017	258.2	±	7.6	264.9	±	10.5	324.0	±	76.7	1.06	97
18KTM1922	25.202	±	0.806	0.0521	±	0.0031	250.9	±	7.9	254.5	±	15.2	288.1	±	140.7	0.79	99
19KTM1922	24.516	±	0.735	0.0514	±	0.0029	257.7	±	7.6	258.0	±	14.7	260.3	±	134.0	0.88	100
20KTM1922	24.582	±	0.713	0.0507	±	0.0015	257.0	±	7.3	254.2	±	9.5	228.4	±	70.8	0.76	101
21KTM1922	25.019	±	0.876	0.0511	±	0.0038	252.6	±	8.7	252.1	±	18.5	247.3	±	180.0	0.76	100
22KTM1922	24.765	±	0.669	0.0512	±	0.0023	255.2	±	6.8	254.8	±	11.8	251.7	±	104.5	0.93	100
23KTM1922	24.716	±	0.692	0.0573	±	0.0020	255.7	±	7.0	281.7	±	11.1	503.7	±	79.0	1.10	91
27KTM1922	24.988	±	0.900	0.0537	±	0.0037	252.9	±	8.9	263.7	±	18.0	360.0	±	161.2	0.71	96
28KTM1922	24.504	±	0.662	0.0519	±	0.0013	257.8	±	6.8	260.0	±	8.5	279.3	±	58.3	0.70	99
29KTM1922	25.349	±	0.760	0.0517	±	0.0020	249.5	±	7.3	251.4	±	11.0	270.0	±	92.0	0.69	99
30KTM1922	24.600	±	0.738	0.0525	±	0.0016	256.9	±	7.6	261.9	±	10.0	306.7	±	72.2	0.68	98
31KTM1922	25.387	±	0.787	0.0511	±	0.0016	249.1	±	7.6	248.7	±	9.8	245.8	±	73.0	0.94	100
32KTM1922	25.176	±	0.780	0.0503	±	0.0019	251.1	±	7.6	247.2	±	10.8	210.3	±	90.6	0.50	102
33KTM1922	25.195	±	0.756	0.0498	±	0.0020	250.9	±	7.4	244.5	±	11.1	183.3	±	98.4	0.90	103

Conc.% = $((^{206}Pb/^{238}U)/(^{207}Pb/^{235}U))*100$

Table 4. Zircon Hf isotopic composition of the Cha Val plutonic rocks

Sample	$^{176}Yb/^{177}Hf$	$^{176}Lu/^{177}Hf$	$^{176}Hf/^{177}Hf$	± 2σ	$^{176}Hf/^{177}Hf$ (t)	$\varepsilon_{Hf}(t)$	± 2σ	T_{DM1} (Ma)	T_{DM2} (Ma)
V1116	15°38'14.1"N, 107°33'06.4"E								
V1116-01	0.053828	0.001511	0.282632	13	0.282623	0.32	0.5	894	1263
V1116-02	0.067487	0.001806	0.282659	15	0.282648	1.23	0.5	862	1206
V1116-03	0.032862	0.000910	0.282601	13	0.282594	-0.68	0.5	923	1327
V1116-04	0.061389	0.001781	0.282639	12	0.282629	0.53	0.4	890	1250
V1116-06	0.087231	0.002444	0.282629	15	0.282615	0.05	0.5	922	1281
V1116-07	0.073669	0.002035	0.282624	14	0.282612	-0.05	0.5	918	1287
V1116-08	0.032498	0.000993	0.282628	13	0.282621	0.27	0.4	887	1267
V1116-09	0.124763	0.003263	0.282708	15	0.282690	2.71	0.5	824	1111
V1116-10	0.019717	0.000599	0.282597	14	0.282592	-0.78	0.5	922	1333
V1116-11	0.067478	0.001852	0.282649	14	0.282638	0.86	0.5	878	1229
V1116-12	0.049694	0.001439	0.282626	15	0.282617	0.13	0.5	900	1275
V1116-13	0.010650	0.000389	0.282619	10	0.282615	0.04	0.4	886	1281
V1116-14	0.039458	0.001224	0.282613	11	0.282605	-0.30	0.4	914	1303
V1116-15	0.036127	0.001059	0.282591	13	0.282584	-1.04	0.5	940	1350
V1116-16	0.052442	0.001462	0.282614	13	0.282605	-0.32	0.4	919	1304
V1116-17	0.086467	0.002374	0.282625	13	0.282611	-0.09	0.5	926	1289
V1116-18	0.039474	0.001111	0.282603	13	0.282595	-0.65	0.5	926	1325
V1116-19	0.052306	0.001506	0.282610	12	0.282600	-0.47	0.4	926	1313
V1116-20	0.049521	0.001458	0.282634	12	0.282625	0.41	0.4	889	1257
V1116-21	0.017734	0.000569	0.282619	12	0.282615	0.03	0.4	889	1282
V1116-22	0.031703	0.000930	0.282598	12	0.282591	-0.79	0.4	928	1334
V1116-23	0.013104	0.000431	0.282611	11	0.282607	-0.25	0.4	898	1299
V1116-24	0.024810	0.000794	0.282616	12	0.282611	-0.11	0.4	899	1291
V1116-25	0.022971	0.000680	0.282595	12	0.282589	-0.86	0.4	926	1338

t = 255 Ma for sample V1116

Table 5. Whole-rock Rb-Sr and Sm-Nd isotopic data of the Cha Val plutonic rocks

Sample	Rb (ppm)	Sr (ppm)	$^{87}Rb/^{86}Sr$	$^{87}Sr/^{86}Sr$ (± 2□)	$(^{87}Sr/^{86}Sr)_i$ (255)	Sm (ppm)	Nd (ppm)	$^{147}Sm/^{144}Nd$	$(^{143}Nd/^{144}Nd)_m$ (± 2□)	$(^{143}Nd/^{144}Nd)_i$	$\varepsilon_{Nd}(t)$	T_{DM2} (Ga)
VN1115	101.4	287.1	1.0225	0.714021 ± 9	0.7103	5.86	33.29	0.18	0.512264 ± 9	0.512086	-4.4	1382
VN1116-1	34.6	278.6	0.3599	0.710535 ± 15	0.7092	4.38	21.88	0.20	0.512332 ± 15	0.512130	-3.5	1313
VN116-2	59.2	60.4	2.8431	0.734757 ± 12	0.7244	1.43	3.76	0.38	0.512296 ± 10	0.512078	-4.5	1394
VN116-3	39.1	513.2	0.2203	0.708908 ± 11	0.7081	4.49	24.79	0.18	0.512345 ± 11	0.512162	-2.9	1262

m: measured isotopic ratios; i: initial isotopic ratios; t = 255 Ma for calculations of initial ratios

Table 6. Ages of Permian-Triassic volcanic and plutonic rocks in Viet Nam. Locations are shown in Fig. 10b

Sample	Rock type	Age (Ma)	Method	Material	Reference
KTM-GbDi1918	Diorite	248.9 ± 1.9	LA-ICP-MS	zircon	This study
KTM-GbDi1921	Diorite	258.0 ± 2.9	LA-ICP-MS	zircon	This study
KTM-Di1922	Diorite	254.0 ± 1.7	LA-ICP-MS	zircon	This study
GO09	Gabbro	250.1 ± 1.5	LA-ICP-MS	zircon	Tran et al. 2020
MLT42	Monzogranite	235 ± 3.1	LA-ICP-MS	zircon	Thanh et al. 2019
MLT34	Monzogranite	242 ± 2.6	LA-ICP-MS	zircon	Thanh et al. 2019
MLT09	Granodiorite	247.4 ± 2.8	LA-ICP-MS	zircon	Thanh et al. 2019
MLT08	Monzogranite	251 ± 3	LA-ICP-MS	zircon	Thanh et al. 2019
V0927	Granite	251.1 ± 3.5	LA-ICP-MS	zircon	Minh et al. 2018
V0926	Granite	251.2 ± 3.8	LA-ICP-MS	zircon	Minh et al. 2018
V0928	Granite	253.9 ± 1.5	LA-ICP-MS	zircon	Minh et al. 2018
V0905	Granodiorite	231 ± 4	LA-ICP-MS	zircon	Hieu et al. 2017
V0903	Granodiorite	233 ± 4	LA-ICP-MS	zircon	Hieu et al. 2017
V1106	Granite	239 ± 6	LA-ICP-MS	zircon	Hieu et al. 2017
V0908	Biotite granite	244 ± 5	LA-ICP-MS	zircon	Hieu et al. 2017
V0821	Tonalite	256 ± 7	LA-ICP-MS	zircon	Hieu et al. 2017
V0741	Granite	260 ± 5	LA-ICP-MS	zircon	Hieu et al. 2017
V0738	Quartz diorite	262 ± 4	LA-ICP-MS	zircon	Hieu et al. 2017
V0856	Granite	263 ± 5	LA-ICP-MS	zircon	Hieu et al. 2017
R11	Rhyolite	256 ± 7	LA-ICP-MS	zircon	Hieu 2017
LH16	Tonalite	234 ± 3.5	LA-ICP-MS	zircon	Wang et al. 2016
LC16	Monzogranite	234.3 ± 1.5	LA-ICP-MS	zircon	Wang et al. 2016
LH13	Tonalite	236.3 ± 3.2	LA-ICP-MS	zircon	Wang et al. 2016
LH11	Tonalite	238.6 ± 3.2	LA-ICP-MS	zircon	Wang et al. 2016
LT4	Granodiorite	240.1 ± 1.6	LA-ICP-MS	zircon	Wang et al. 2016
LH4	Granodiorite	244.5 ± 2	LA-ICP-MS	zircon	Wang et al. 2016
LT6	Granodiorite	244.8 ± 3.9	LA-ICP-MS	zircon	Wang et al. 2016
LC1	Monzogranite	245.1 ± 2.9	LA-ICP-MS	zircon	Wang et al. 2016
LC8	Monzogranite	245.9 ± 2.8	LA-ICP-MS	zircon	Wang et al. 2016
LH1	Granodiorite	249 ± 1.9	LA-ICP-MS	zircon	Wang et al. 2016
LH5	Granodiorite	249.9 ± 1.8	LA-ICP-MS	zircon	Wang et al. 2016
LC17	Monzogranite	251.2 ± 2.1	LA-ICP-MS	zircon	Wang et al. 2016
LC12	Monzogranite	253.3 ± 1.8	LA-ICP-MS	zircon	Wang et al. 2016
LT1	Granodiorite	254.4 ± 2.5	LA-ICP-MS	zircon	Wang et al. 2016
LC6	Monzogranite	254.9 ± 1.6	LA-ICP-MS	zircon	Wang et al. 2016
LT3	Granodiorite	256.4 ± 3.1	LA-ICP-MS	zircon	Wang et al. 2016
V1102-3	Granite	224 ± 4.6	LA-ICP-MS	zircon	Hieu et al. 2015
V1102	Granite	234.7 ± 3.7	LA-ICP-MS	zircon	Hieu et al. 2015
V1124	Granite	235 ± 14	LA-ICP-MS	zircon	Hieu et al. 2015
V1127	Granite	241.4 ± 2	LA-ICP-MS	zircon	Hieu et al. 2015
V1125	Granite	242.1 ± 4.8	LA-ICP-MS	zircon	Hieu et al. 2015
V1114	Granite	242 ± 2.4	LA-ICP-MS	zircon	Hieu et al. 2015
VN12-066	Granodiorites	242.2 ± 1.3	LA-ICP-S	zircon	Shi et al. 2015
VN12-050	Plagiogranite	251.8 ± 1.9	LA-ICP-MS	zircon	Shi et al. 2015
VN12-025	Rhyolite	251.9 ± 1.7	LA-ICP-MS	zircon	Shi et al. 2015
VN12-022	Monzogranite	253.4 ± 1.5	LA-ICP-MS	zircon	Shi et al. 2015
VN12-056	Monzogranites	260.9 ± 1.6	LA-ICP-MS	zircon	Shi et al. 2015
LTH26A	Granite	248.7 ± 6.9	LA-ICP-MS	zircon	Usuki et al. 2015
LB19A	Ryholite	251.5 ± 5.0	LA-ICP-MS	zircon	Usuki et al. 2015
YB27	Granite	252.3 ± 5.2	LA-ICP-MS	zircon	Usuki et al. 2015
LTH9	Granite	252.8 ± 7.7	LA-ICP-MS	zircon	Usuki et al. 2015
YB24	Granite	253.0 ± 2.4	LA-ICP-MS	zircon	Usuki et al. 2015

Sample	Rock type	Age (Ma)	Method	Material	Reference
YB21	Ryholite	253.2 ± 2.5	LA-ICP-MS	zircon	Usuki et al. 2015
BK6	Granite	253.3 ± 2.6	LA-ICP-MS	zircon	Usuki et al. 2015
YB29	Granite	253.7 ± 2.5	LA-ICP-MS	zircon	Usuki et al. 2015
YB12	Ryholite	254.6 ± 2.6	LA-ICP-MS	zircon	Usuki et al. 2015
PSP37	Granite	256.3 ± 6.0	LA-ICP-MS	zircon	Usuki et al. 2015
LTH21A	Granite	257.7 ± 3.7	LA-ICP-MS	zircon	Usuki et al. 2015
LTH81-3	Ryholite	257.9 ± 3.3	LA-ICP-MS	zircon	Usuki et al. 2015
LTH82	Ryholite	258.3 ± 3.2	LA-ICP-MS	zircon	Usuki et al. 2015
LTH12	Granite	259.0 ± 3.5	LA-ICP-MS	zircon	Usuki et al. 2015
LTH77	Ryholite	259.1 ± 3.2	LA-ICP-MS	zircon	Usuki et al. 2015
LTH76A	Ryholite	259.7 ± 3.1	LA-ICP-MS	zircon	Usuki et al. 2015
LTH76B	Ryholite	259.8 ± 3.1	LA-ICP-MS	zircon	Usuki et al. 2015
LTH81-1	Ryholite	261.9 ± 3.5	LA-ICP-MS	zircon	Usuki et al. 2015
JH0804	Granitic gneiss	244.5 ± 2.5	LA-ICP-MS	zircon	Tran et al. 2014
JH0822	Granite	245.9 ± 1.5	LA-ICP-MS	zircon	Tran et al. 2014
JH0810	Granodiorite	252.1 ± 1.5	LA-ICP-MS	zircon	Tran et al. 2014
KD10-32/1	Diorite	255.6 ± 3.4	LA-ICP-MS	zircon	Tran et al. 2014
DCL09	Dioritic gneiss	257.2 ± 4.4	LA-ICP-MS	zircon	Tran et al. 2014
VT 225	Granite	225 ± 3	LA-ICP-MS	zircon	Roger et al. 2014
VT 226	Granite	230 ± 1	LA-ICP-MS	zircon	Roger et al. 2014
V0783	Granite	251.0 ± 2.0	LA-ICP-MS	zircon	Hieu et al. 2013
V0779	Granite	253.0 ± 2.0	LA-ICP-MS	zircon	Hieu et al. 2013
V0789	Granite	251.0 ± 2.0	LA-ICP-MS	zircon	Hieu et al. 2013
V0786	Granite	253.0 ± 2.0	LA-ICP-MS	zircon	Hieu et al. 2013
MH	Granite	260.0 ± 3.0	SHRIMP	zircon	Anczkiewicz et al. 2013
11SM5I	Eclogite	230.5 ± 8.2	SHRIMP	zircon	Zhang et al. 2013
V0829	Quartz diorite	270.9 ± 3.3	LA-ICP-MS	zircon	Liu et al. 2012
	Granite	260 ± 4	SHRIMP	zircon	Hoa et al. 2008
VN 09	Gneiss	244 ± 7	SHRIMP	zircon	Carter et al. 2001

Whole-rock Sr and Nd isotopes were analyzed at the Institute of Geology and Geophysics, Chinese Academy of Sciences, Beijing. About 100 mg of rock powder from each sample was dissolved with a mixture of distilled HF-$HClO_4$ solution using Teflon beakers in steel-jacketed vessels at 180°C for six days to ensure complete dissolution. Sm and Nd were separated by conventional ion-exchange techniques and their isotopic ratios were measured by using a Finnigan MAT-262 mass spectrometer. Isotopic ratios were corrected for mass fractionation by normalizing to 0.7219 for $^{146}Nd/^{144}Nd$ and $^{86}Sr/^{88}Sr = 0.1194$. Total procedure blanks are <500 pg for Nd, <500 pg for Sr, and <100 pg for Sm. The standard NBS-607 Sr and BCR-1 Nd gave $^{87}Sr/^{86}Sr = 1.20042 \pm 2$ and $^{143}Nd/^{144}Nd = 0.512604 \pm 7$, respectively. Detailed analytical procedures are shown in (Chen et al., 2000; 2007). The analytical results are presented in Table 5.

4. Analytical results

4.1. Geochemistry

A total of eleven samples from Cha Val plutonic rocks were analyzed for major and trace element compositions. Geochemical results are shown in Tables 1 and 2 with SiO_2 content ranging from 51.88 to 67.93 wt%, Al_2O_3 from 10.91 to 18.89 wt%, Na_2O+K_2O from 2.99 to 6.32 wt%, and a wide range of Na_2O/K_2O ratios (1.58-3.23). The loss on ignition ranges from 0.78 to 4.88 wt%. Most of the samples fall into the diorite field and few of them point to the granodiorite field (Fig. 3a). The A/CNK ratios of 0.49-0.91 plot in the metaluminous field except for sample V1115 falling into a peraluminous field (high

K-feldspar) (Fig. 3b). The K_2O composition ranges from 1.16 to 2.40 wt% and belongs to the medium to high K affinity (Fig. 3c). According to the granitic classification scheme, all samples plot in I-type granite field (Fig. 3d). Most of the samples follow the trend for I-type granite on the P_2O_5 vs SiO_2 and Y vs Rb diagrams (Fig. 3e, f). Calculation of CIPW norm exhibits an assemblage of quartz, plagioclase, K-feldspar, and hypersthene, which is compatible with the petrographical observations.

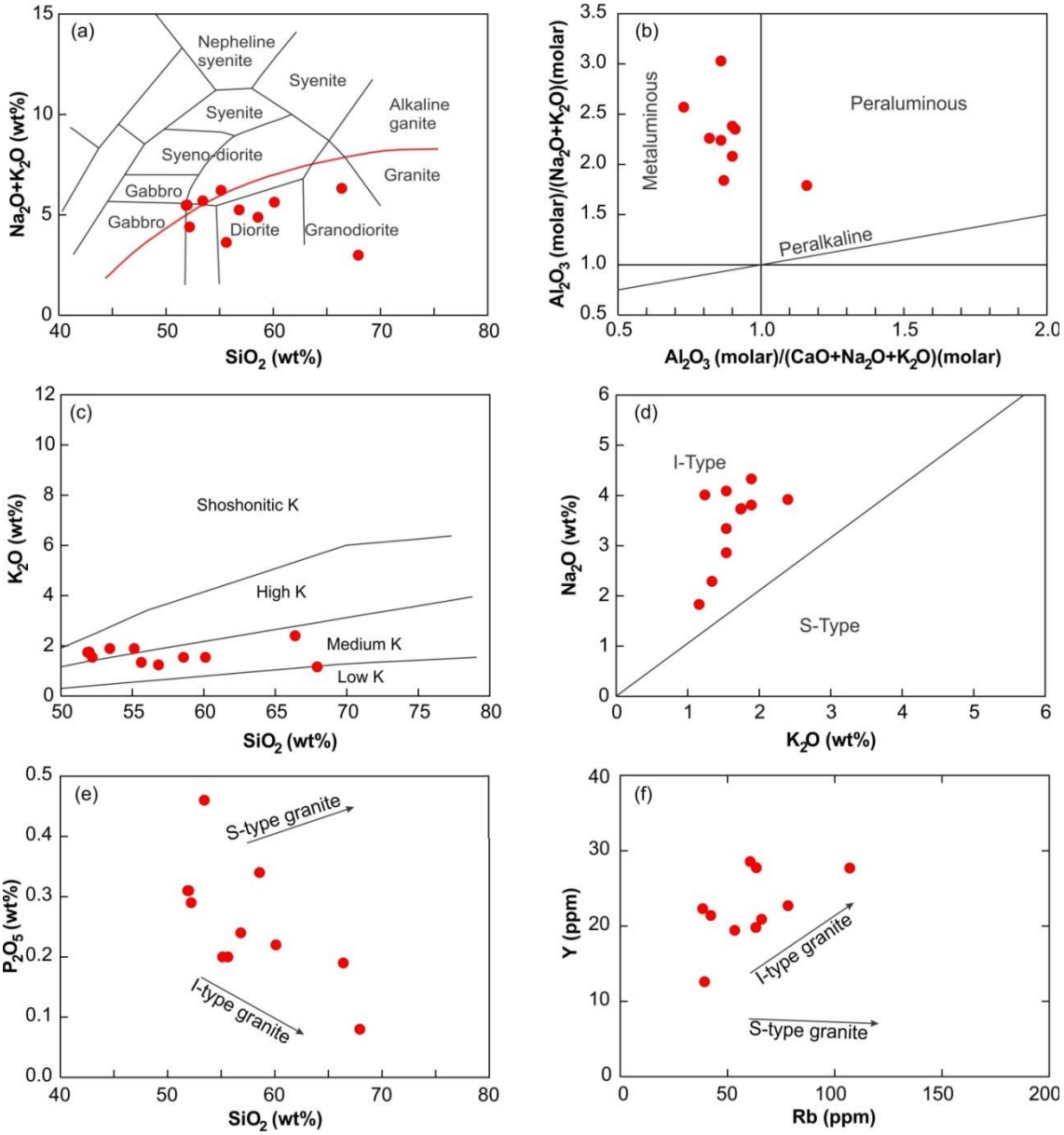

Figure 3. Classification diagrams of the Cha Val plutonic rocks: (a) TAS diagram (Middlemost, 1994); (b) A/CNK vs A/NK diagram Maniar and Piccoli, 1989; (c) K_2O vs SiO_2 diagram (Peccerillo and Taylor, 1976); (d) Granite type discrimination (Chappell and White, 1974); and (e, f) The trend of I- and S-type granites (Chappell, 1999)

The total rare earth element compositions (∑REE) of the Cha Val plutonic rocks range from 25.53 to 205.61 ppm. These samples indicate enrichment of light rare earth elements (∑LREE = 14.86-187.19 ppm) and depletion of heavy rare earth elements (∑HREE = 0.86-18.42 ppm). Chondrite-normalized REE patterns are characterized by a moderate negative anomaly of Eu (Eu/Eu* = 0.62-0.95) and show a fractionated REE pattern (Fig. 4a). Primitive mantle-normalized multi-element diagram indicate enrichment in Cs, U, K, Pb, and Nd but depletion in Ba, Nb, Ta, P, and Ti (Fig. 4b). The negative anomalies observed for Eu and Ba are probably due to the fractional crystallization of plagioclase and K-feldspar. Zircon saturation thermometer of Watson and Harrison (1983) is used to estimate the crystallization temperature (T_{Zr}(°C)) of the Cha Val plutonic rocks and gave a range of 600-838°C. On the P_2O_5 vs SiO_2 diagrams, samples plot in a similar temperature range of 65-850°C (Fig. 5a). According to the tectonic classification of ferroan versus magnesian affinities (Frost et al., 2001), samples dominantly fall into the cordilleran granitoid field (Fig. 5b). On the tectonic environment diagram after Pearce et al. (1984), they are restricted in the volcanic arc granite field (Figs. 5c,d).

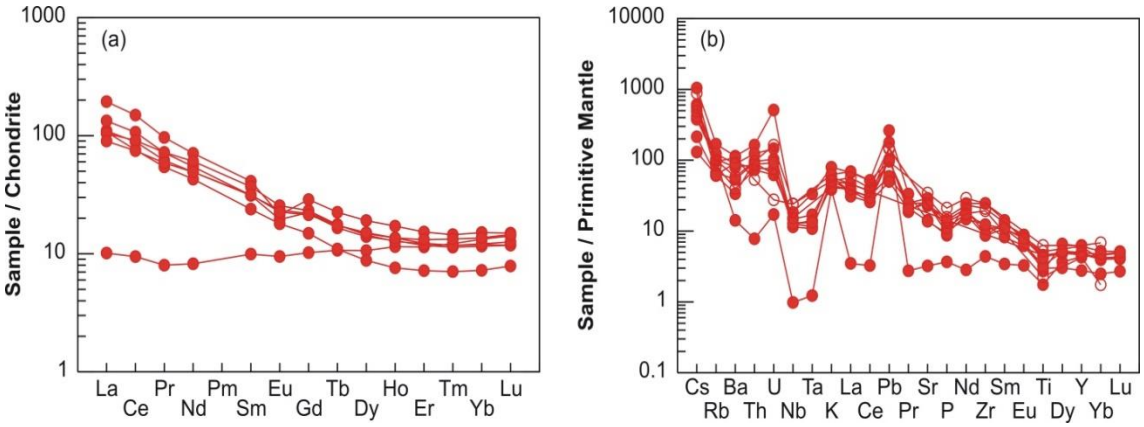

Figure 4. (a) Chondrite-normalized REE patterns and (b) primitive mantle-normalized multi-element patterns for the Cha Val plutonic rocks. Normalization values are from Sun and McDonough (1989)

4.2. Zircon U-Pb geochronology

Representative cathodoluminescence (CL) images of the three samples (KTM-GbDi1918, KTM-GbDi1921 and KTMDi1922) from the Cha Val plutonic rocks of dioritic composition are shown in Fig. 6. The zircon grains of the analyzed samples are mostly euhedral, transparent, ranging from 100 to 250 μm in size with width to length ratios of 1:2-1:3. Their CL images display oscillatory zoning typical for magmatic zircon. The LA-ICP-MS U-Pb zircon dating results with a total of 62 spots are presented in Fig. 7 and Table 3. These zircon grains are characterized by high Th/U ratios of 0.23-1.3 (> 0.1) which are typical feature of the magmatic zircon (Hoskin and Schaltegger, 2003). Almost all dating results are plotted on Wetherill concordia diagrams and show a narrow age range of Permian-Triassic ($^{206}Pb/^{238}U$ age of 279-238 Ma). Several zircon grains plot below concordia curve, indicating progressive loss of radiogenic lead.

Sample KTM-GbDi1918 (Coordinate: 15°38'26.1"N, 107°34'11.5"E): Twenty zircon grains from this sample were selected for LA-ICP-MS analysis. Zircon $^{206}Pb/^{238}U$ ages vary from 241.6 to 279.4 Ma. Seventeen analyzed spots yielded a weight mean $^{206}Pb/^{238}U$ age of 248.9 ± 1.9 Ma (MSWD = 0.92, n = 17) (Fig. 7a), representing the crystallization age of dioritic sample KTM-GbDi1918 in the Early Triassic.

Sample KTM-GbDi1921 (Coordinate: 15°35'16.5"N, 107°30'06.3"E): Twenty-one zircon grains from this sample were selected for LA-ICP-MS analysis. Zircon $^{206}Pb/^{238}U$ ages vary from 238.4 to 272.9 Ma. Twenty analyzed spots yielded a weight mean $^{206}Pb/^{238}U$ age of 258.0 ± 2.9 Ma (MSWD = 2.0, n = 20) (Fig. 7b), representing the crystallization age of dioritic sample KTM-GbDi1921 in the Late Permian.

Sample KTM-Di1922 (Coordinate: 15°37'42.7"N, 107°32'35.0"E): Twenty-one zircon grains from this sample were selected for LA-ICP-MS analysis. Zircon $^{206}Pb/^{238}U$ ages vary from 249.1 to 261.1 Ma. Nineteen analyzed spots yielded a weight mean $^{206}Pb/^{238}U$ age of 254.0 ± 1.7 Ma (MSWD = 1.03, n = 19) (Fig. 7c), representing the crystallization age of dioritic sample KTM-Di1922 in the Late Permian.

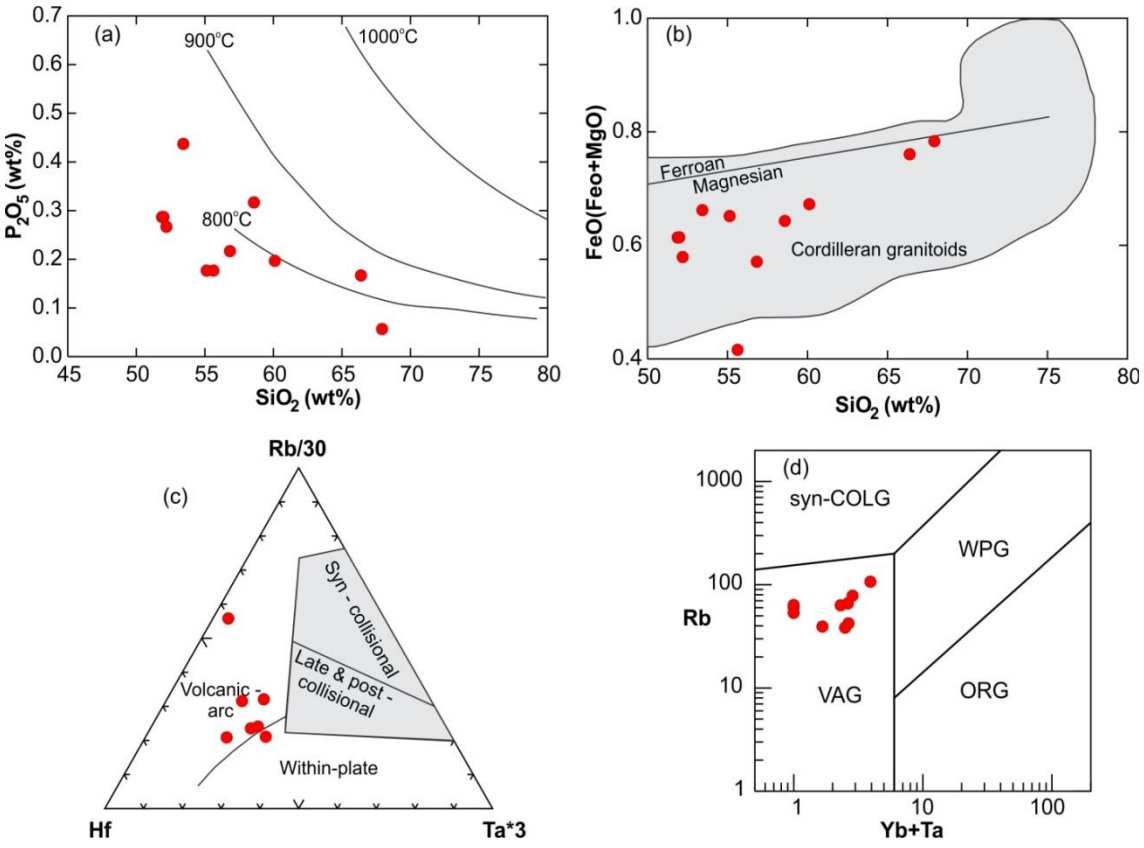

Figure 5. (a) P_2O_5-SiO_2 temperature (Watson and Harrison, 1984); (b) FeO/(FeO+MgO)-SiO_2 diagrame (Frost et al., 2001); (c) Rb/30-Hf-T*3 discrimination (Harris et al., 1986); and (d) Geotectonic discrimination (Pearce et al., 1984)

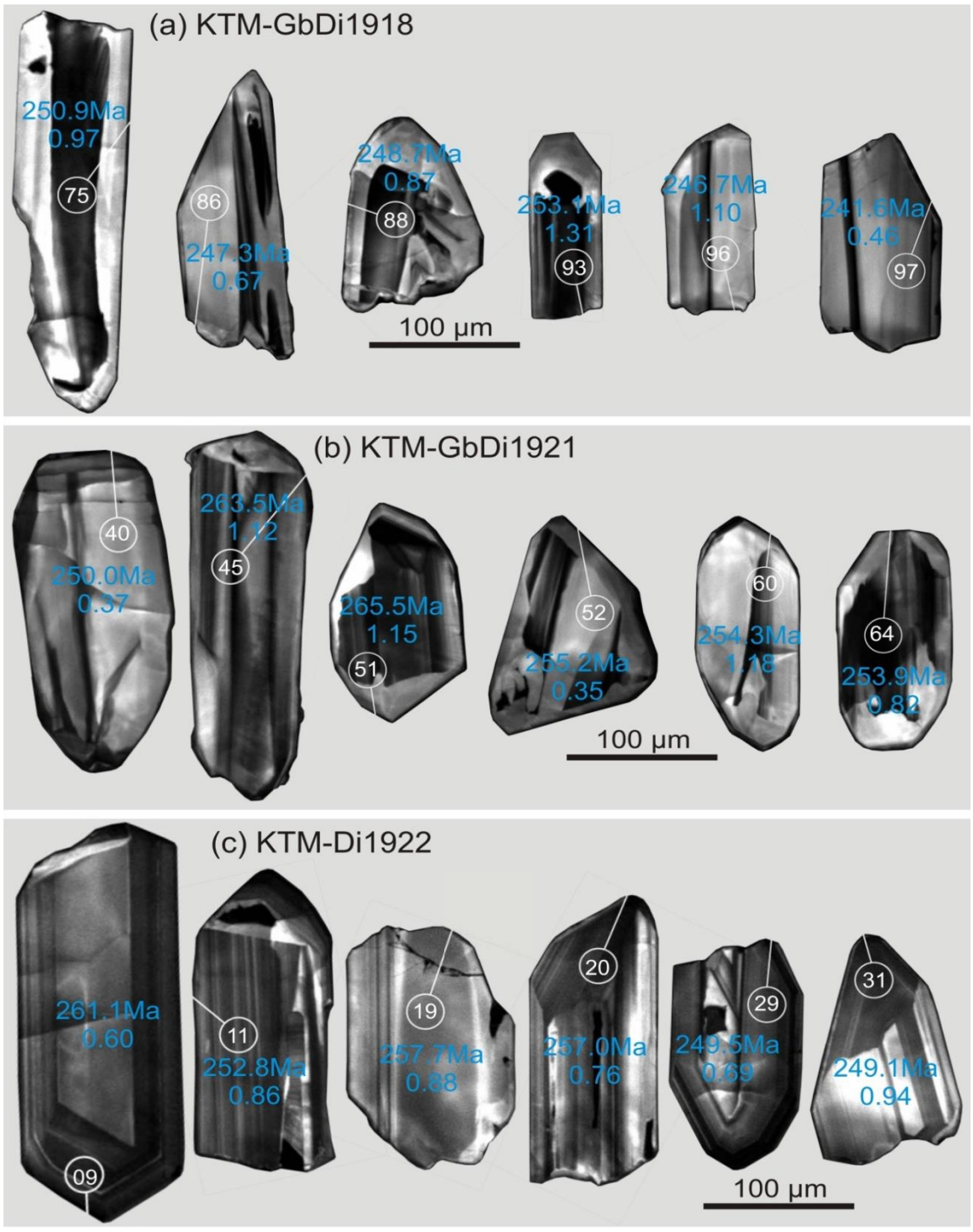

Figure 6. Cathodoluminescence (CL) images of representative zircon grains from the Cha Val magmatic rocks

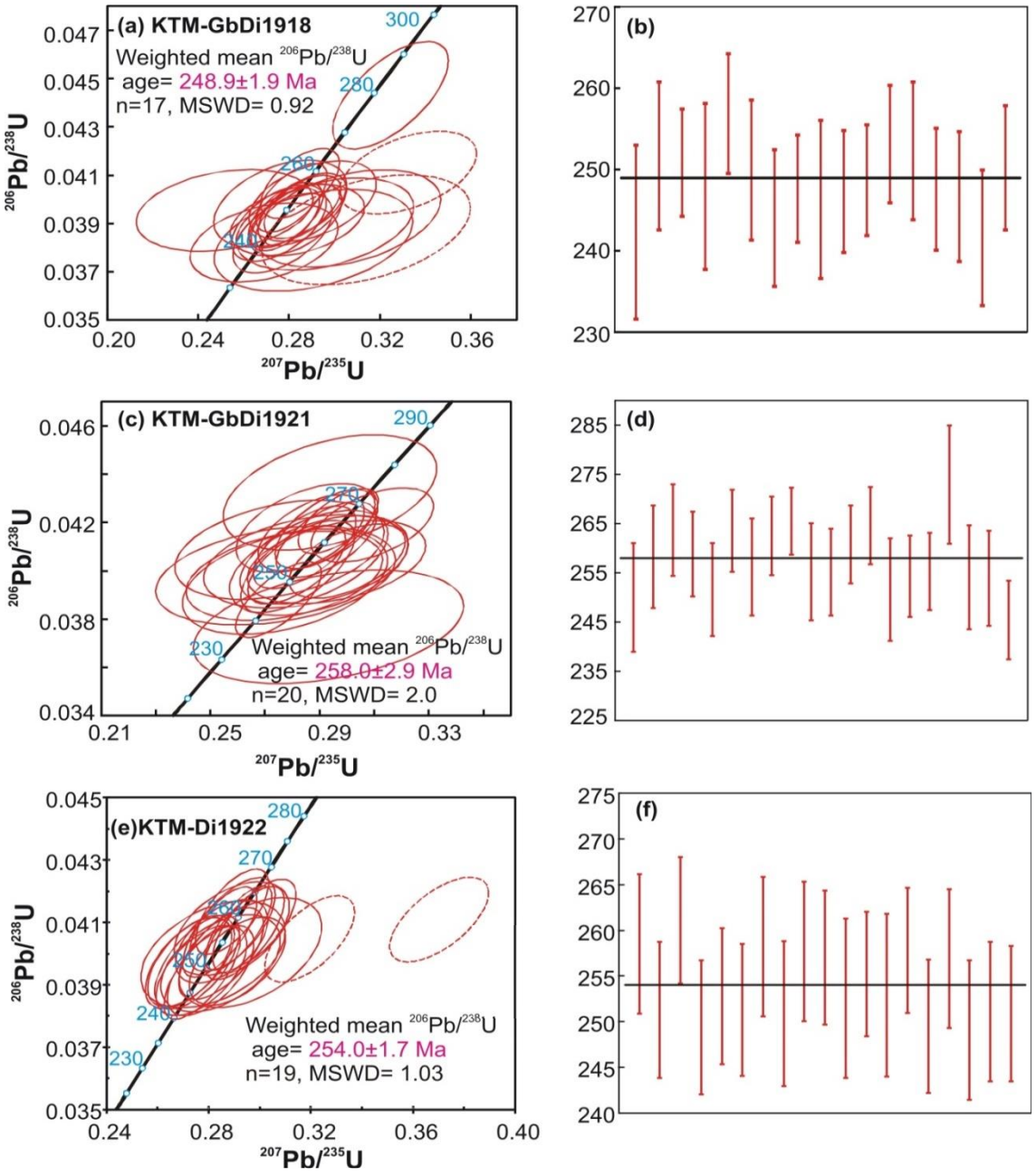

Figure 7. Zircon LA-ICP-MS U-Pb concordia and weighted mean diagrams of the Cha Val plutonic rocks

4.3. Sr-Nd-Hf isotopic composition

Twenty-four zircon grains from dioritic sample V1116 of Cha Val plutonic rocks were selected for Lu-Hf isotope analyses. The zircon Lu-Hf isotope results are shown in Table 4 and Fig. 8. The $\varepsilon_{Hf}(t)$ values, calculated using the representative age of 255 Ma on the basis of the zircon U-Pb ages, range from -1.04 to +2.71 with a weighted mean value of 0.0 ± 1.0 (MSWD=0.102) (Fig. 8a). The initial $^{176}Hf/^{177}Hf$ ratios of

dioritic sample V1116 range from 0.282584 to 0.282690. The measured $^{176}Lu/^{177}Hf$ ratios vary from 0.000389 to 0.003263. Their zircon Hf model ages (T_{DM2}) indicate a range of 1111-1350 Ma with a weighted mean value of 1283 ± 21 Ma (MSWD=4.1) (Fig. 8b). The Hf isotopic signatures of the Cha Val plutonic rocks suggest that they were derived from partial melting of Mesoproterozoic crustal rocks with a contribution of a minor extent of mantle-derived components.

The Rb-Sr and Sm-Nd isotopic data of the Cha Val plutonic rocks are presented in Table 5. The negative $\varepsilon_{Nd}(t)$ values from -4.5 to -2.9 (weighted mean value of -3.8) were calculated from the whole-rock Sr-Nd isotopic compositions at the age of 255 Ma (Fig. 9), consistent with I-type granites in the LFB. Their initial $^{87}Sr/^{86}Sr$ and $^{143}Nd/^{144}Nd$ ratios respectively range from 0.7081 to 0.7244 and from 0.512078 to 0.512162. Their whole-rock two-stage model ages (T_{DM2}) show a range of 1394-1262 Ma with a weighted average value of 1338 Ma. Hence, the Nd isotopic signatures of the Cha Val plutonic rocks, suggest that they were derived from partial melting of Mesoproterozoic crustal rocks with a contribution of a minor extent of mantle-derived components.

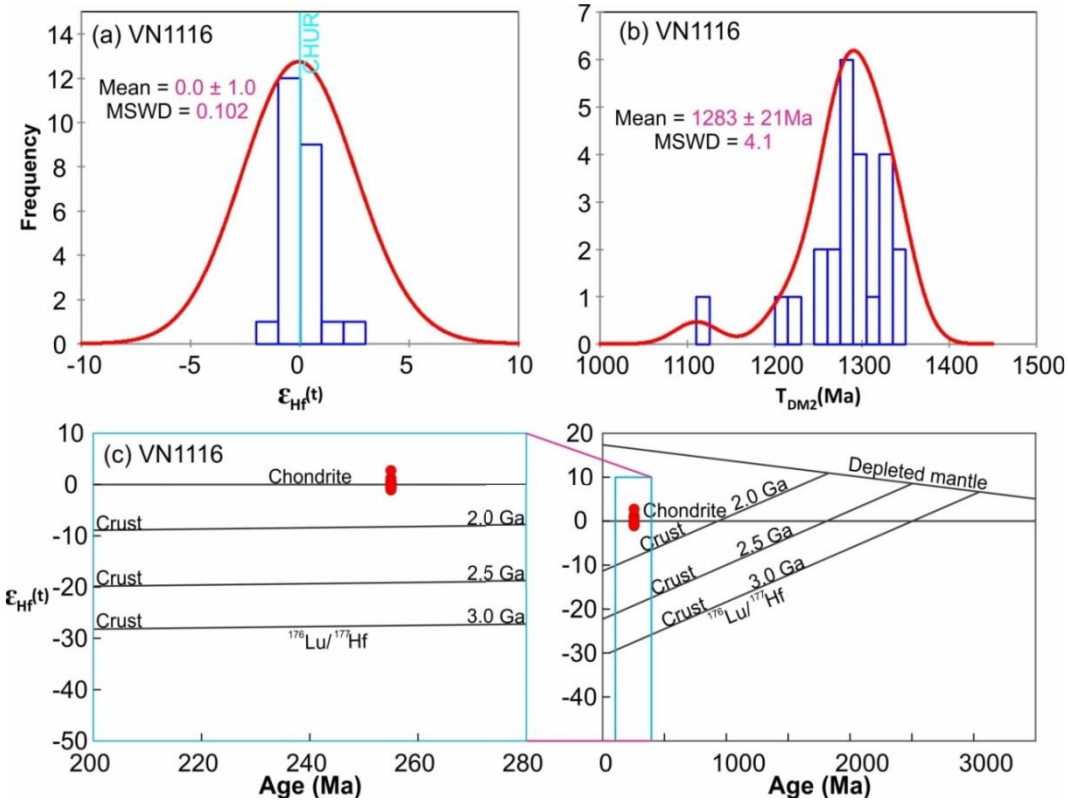

Figure 8. (a) Histograms of zircon $\varepsilon_{Hf}(t)$ values and (b) zircon Hf isotope model age (T_{DM2}) from the Cha Val plutonic rocks5. Discussions

5.1. Emplacement age

Recently, the Cha Val plutonic rocks have been dated using different methods. According to the geological relationships with the surrounding rocks (Trang, 1994), they intrude Early Cambrian-Middle Ordovician sediments and are, in turn, intruded by the Middle-Late Triassic Hai Van two-mica

granites. Additionally, age dating results using K-Ar method on plagioclase gave a weighted mean age of 243±3 Ma (Tri and Khuc, 2011). Hence, they are interpreted as the plutonic rocks emplaced during the Late Permian-Early Triassic time. Recently, Tran et al. (2020) reconstructed the history of stratigraphic-tectonic evolution in Indochina and surrounding areas, in which, the gabbro sample from Cha Val plutonic rocks was dated at 250.2±2.1 Ma using LA-ICP-MS zircon U-Pb method.

In this study, we analyzed three samples of the Cha Val plutonic rocks of dioritic composition with LA-ICP-MS U-Pb zircon ages and the obtained results yielded a narrow age range of 258 to 249 Ma. This Late Permian-Early Triassic age range is interpreted as the emplacement age of the Cha Val plutonic rocks. This timing is similar to that of Tran et al. (2020) and indicates that the crystallization age of the Cha Val plutonic rocks lasted at least for about 10 Myr. The emplacement age of the Cha Val plutonic rocks (258-249 Ma) was younger than that of Ben Giang-Que Son rocks (294 Ma, Sang, 2011).

5.2. Petrogenesis

According to the classification system of I, S-, A-type granites, the Cha Val plutonic rocks in the study area show the trend typical for I-type granite. In the field, the Cha Val rocks do not contain metasedimentary xenoliths of ancient geological formations. Considering the classification system of granitic rocks of Barbarin, 1999), the mineral assemblages of the Cha Val plutonic rocks are characterized as rich in hydrous minerals such as hornblende and biotite, while aluminum-rich minerals such as muscovite and cordierite are absent in rock compositions (Fig. 2), in which characteristic for I-type affinity. In terms of geochemical characteristics, the Cha Val plutonic rocks show low SiO_2 and high Fe_2O_3, MgO, and CaO compositions, and are categorized as the metaluminous type with an average A/CNK value of 0.85 (Fig. 3b). The composition of Na_2O is higher than that of K_2O, similar to I-type granite (Fig. 3c, d). Moreover, on the SiO_2-P_2O_5 and Rb-Y diagrams, the Cha Val plutonic samples follow the I-type trends (Fig. 3e, f). In chondrite- and primitive mantle-normalized diagrams (Fig. 4), Cha Val plutonic samples display enrichment in Cs, U, Pb, and Nd and depletion in Ba, Nb, Ta, P, Eu, and Ti, which may indicate fractional crystallization of common minerals (e.g., plagioclase, K-feldspar, apatite, and biotite).

The zircon saturation (Watson and Harrison, 1983) and apatite saturation thermometry (Watson and Harrison, 1983) show that the Cha Val plutonic rocks were formed at 600°C-850°C (Table 2 and Fig. 5a). They are generated by the volcanic-arc environment (Figs. 5c, d). The CL zircon images (Fig. 6) are characterized by the absence of xenocrystic zircons and the LA-ICP-MS isotopic results have no significant older inherited dates. With those, they may indicate that zircons have crystallized in a single geological event. In terms of isotope composition, the Cha Val plutonic rocks display a relatively narrow range of $^{87}Sr/^{86}Sr$ ratio (0.7081 to 0.7244) and $^{143}Nd/^{144}Nd$ ratio (0.512078 to 0.512162). They have a the relatively restricted zircon $\varepsilon_{Hf}(t)$ values (-1.04 to 2.71), negative whole-rock $\varepsilon_{Nd}(t)$ values (-4.5 to -2.9), and whole-rock Nd and zircon Hf model ages (T_{DM2}) of the Mesoproterozoic time (1394-1111 Ma) (Figs. 8a, b and 9a). These observations suggest that the Cha Val plutonic rocks were likely generated from the melting of Mesoproterozoic crustal materials with a minor contribution of mantle-derived components (Figs. 8c and 9).

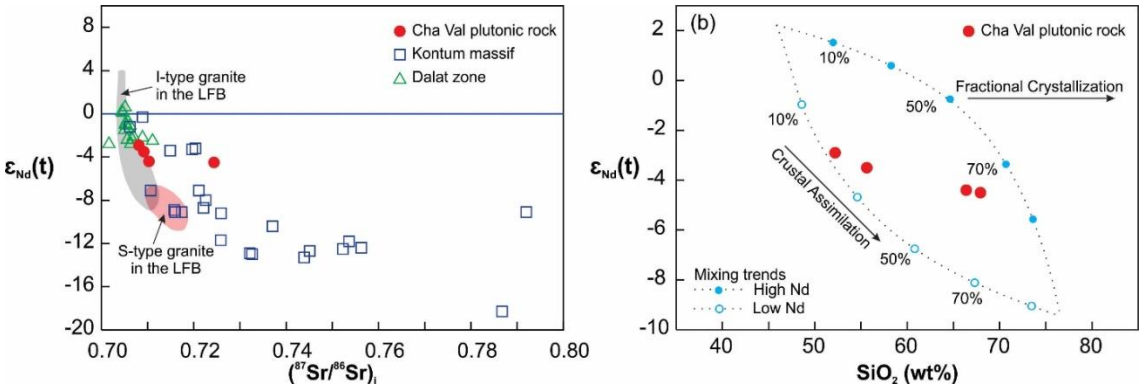

Figure 9. Whole-rock Rb-Sr and Sm-Nd radiogenic isotope results of the Cha Val plutonic rocks. I-and S-type granites in Lachlan Fold Belt (LFB) are from Healy et al. (2004). Data obtained in this study and compiled from Lan et al. (2003); Owada et al. (2007); Shellnutt et al. (2013)

5.3. Genetic correlation of the Cha Val plutonism and Permian-Triassic regional tectonic events

Previous studies on magmatic activities related to the subduction and closure of the Paleo-Tethys ocean during the Late Permian-Early Triassic in the Vietnamese territory have basically given an overall view of their formation timing, origin, and tectonic setting (Figs. 10 and 11) (Thuc and Trung, 1995; Carter et al., 2001; Hoa et al., 2008; Liu et al., 2012; Żelaźniewicz et al., 2013; Hieu et al., 2013; 2015; 2017; Zhang et al., 2013; Tran et al., 2014; Roger et al., 2014; Shi et al., 2015; Usuki et al., 2015; Wang et al., 2016; Minh et al., 2018; Thanh et al., 2019; Nakano et al., 2021). Figure 10b displays the widespread distribution of granitic magmas in north-central Vietnam during the Late Permian-Early Triassic, which can be divided into three major NW-SE-trending geological regions belonging to the two tectonic settings (intra-continental rift and subduction): (1) the Phan Si Pan zone, Tu Le basin and Song Da rift, (2) the northern Truong Son belt and Song Ma suture, and (3) the southern Truong Son belt and north Kontum massif.

(1) The Phan Si Pan zone and Tu Le basin in Northwest Vietnam (Fig. 10b) comprises A-type granites (Ye Yen Sun granite, Nam Xe-Tam Duong granite, Muong Hum granite, Phu Sa Phin granite, Phan Si Pan granite) and Tu Le rhyolite, and the Song Da intraplate rift with a dominance of Permian basalts.

These Permian-Triassic volcanic-plutonic assemblages are possibly produced by the Emeishan mantle plume event between 261.9 and 248.7 Ma (section AB, Fig. 11b) (Anczkiewicz et al., 2012; Hieu et al., 2013; Tran et al., 2015; Minh et al., 2018). The A-type granites in this area are characterized by the presence of alkaline minerals (aegirine, riebeckite, and arfvedsonite) and positive $\varepsilon_{Hf}(t)$ values (+1.9 to +15.9) (Hieu et al., 2013; Usuki et al., 2015; Minh et al., 2018). The low- to high-Ti signature and widespread extent of ultramafic-mafic rocks of the Song Da intraplate rift are similar to those of the Emeishan mantle plume (Tran et al., 2016).

(2) The northern Truong Son belt and Song Ma suture (Fig. 10b) are composed of I-type granites (Chieng Khuong granite, Song Ma granite, and Dien Bien granite) which are products of Paleo-Tethys subduction beneath the Indochina blocks along the Song Ma suture during the Late Permian-Early Triassic (section AB, Fig. 11b) (Carter et al., 2001; Liu et al., 2012; Vượng et al., 2013; Shi et al., 2015; Wang et al., 2016; Hieu et al., 2017) (Fig. 10b).

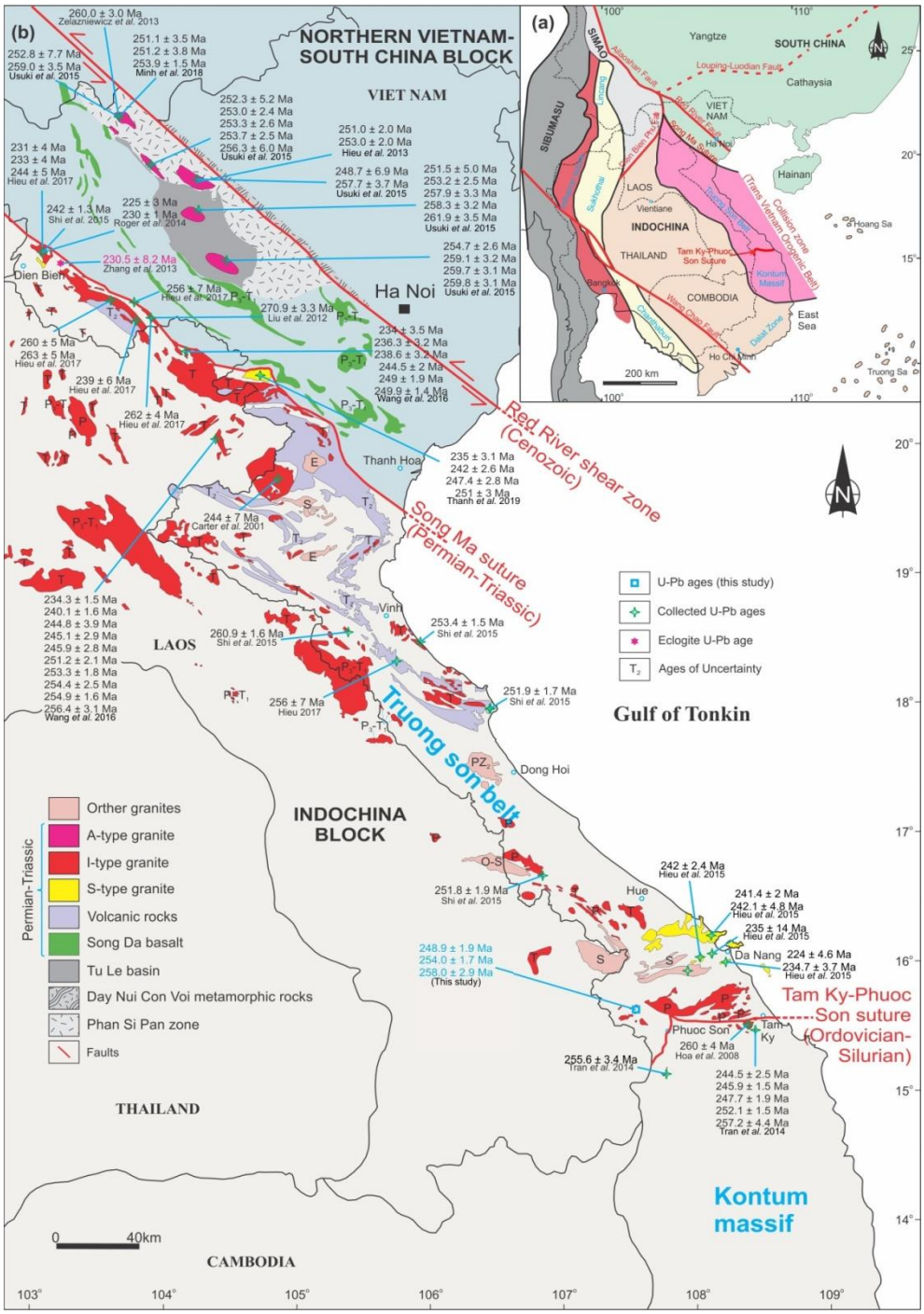

Figure 10. (a) Tectonic sketch of central and eastern Asia and (b) Simplified geological map of the Indochina block showing emplacement ages of Permian-Triassic rocks (data obtained in this study and compiled from Carter et al., 2001; Hoa et al., 2008; Liu et al., 2012; Żelaźniewicz et al., 2013; Hieu et al., 2013; 2015; 2017; Zhang et al., 2013; Tran et al., 2014; Roger et al., 2014; Shi et al., 2015; Wang et al., 2016; Minh et al., 2018; Thanh et al., 2019)

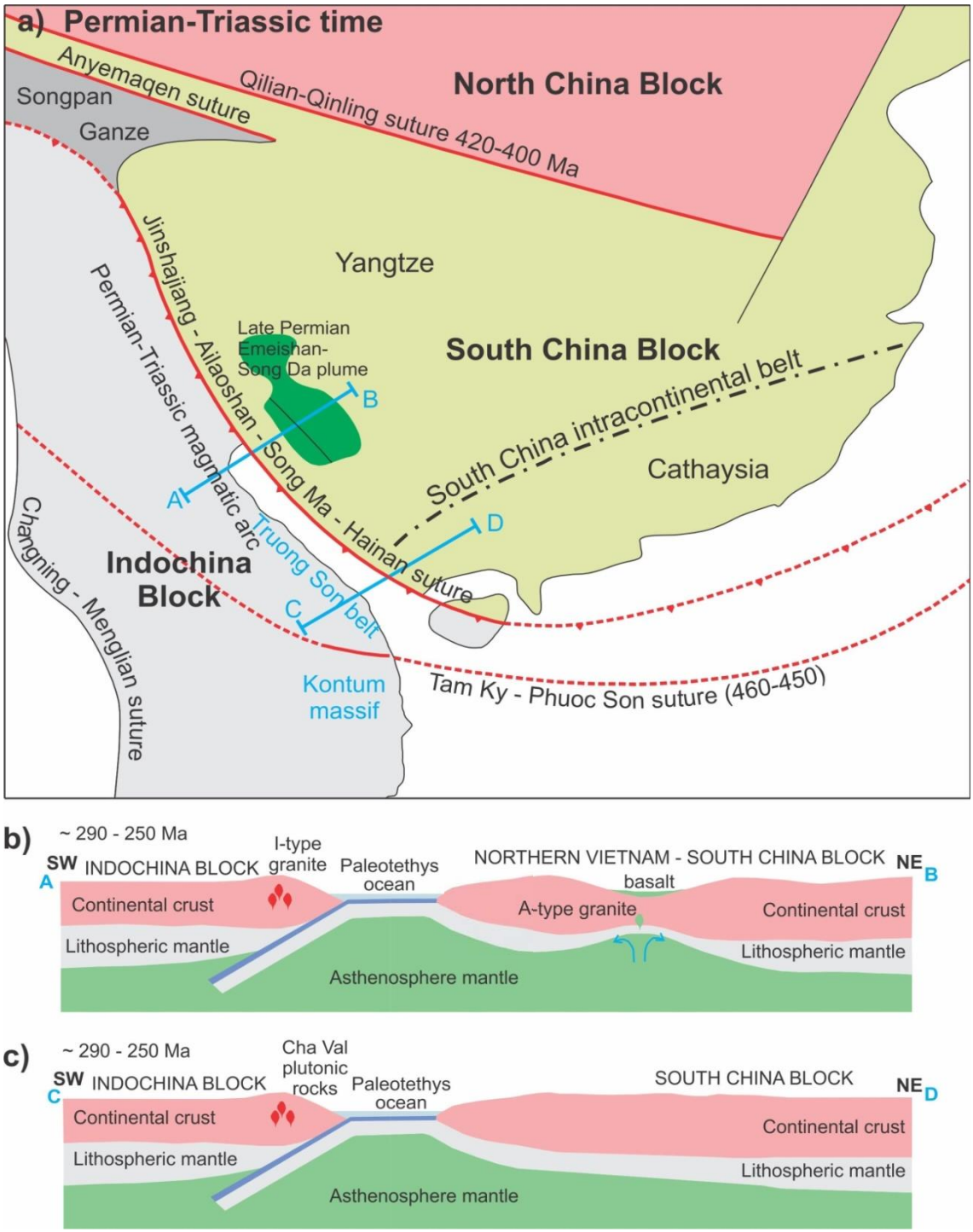

Figure 11. (a) Tectonic reconstruction of the Indochina block and its adjacent areas in Permian-Triassic (Faure et al., 2018) and (b) Tectonic setting for the Cha Val plutonic rocks and other Permian-Triassic magmas in Vietnam

(3) In the southern Truong Son belt and north Kontum massif, central Vietnam (Fig. 10b), Ben Giang granites have also been suggested to genetically connect with the subduction of the Paleo-Tethys ocean beneath the Indochina blocks (CD section, Fig. 11c) (Hoa et al., 2008; Sang, 2011; Tran et al., 2014; Nakano et al., 2021). This subduction took place in central Vietnam, especially in Kontum massif, and is evidenced by the occurrence of abundant Late Permian-Early Triassic granitic formations (e.g., 250 Ma; Owada et al., 2007 and 257-244 Ma; Tran et al., 2014).

The origin and formation mechanism triggering magmatism of metaluminous I-type affinity was suggested by Barbarin (1999), who classified granitoids based on the Wilson cycle, to link with two main tectonic settings: (1) magmatism associated with an Andean-type continental arc and (2) post-orogenic lithospheric extension. In this study, the Cha Val plutonic rocks are metaluminous I-granite and associated with subduction-related magmatism (Figs. 3, 5, 8, and 9). The U-Pb isotopic age (258-249 Ma) of the Cha Val plutonic rocks in the southern Truong Son belt (Fig. 7) and the I-type granites in the northern Truong Son belt are coincident with widespread magmatism. According to the above results, the Cha Val plutonic rocks document the pre-collisional magmatism related to the south-directed subduction of the Paleotethys (Fig. 10a) (Osanai et al., 2008) and cluster along a Permian-Triassic magmatic arc (Fig. 11a) (Faure et al., 2018). The I-type granites of the Cha Val plutonic rocks contribute to the building of the active continental margin of Indochina, and hence, are incorporated into this Permian-Triassic magma arc. With all the above original characteristics and formation timing, they can be presumably interpreted to form in the subduction stage (290-250 Ma) of the Paleo-Tethys ocean beneath the Indochina block along the Song Ma suture (Fig. 11a, c).

6. Conclusions

Petrography, whole-rock geochemistry, zircon U-Pb geochronology, and Sr-Nd-Hf isotopic composition of the Cha Val plutonic rocks allow us to reach the following conclusions:

The Cha Val plutonic rocks in the southern part of the Truong Son belt are composed mainly of diorite, quartz diorite and granodiorite. Major mineral compositions include plagioclase, hornblende, quartz, biotite, and K-feldspar. They are characterized by low to medium SiO_2 content, low A/CNK, and $Na_2O/K_2O > 1$, and correspond to I-type granite originated from an Andean-type continental arc.

The Sr-Nd-Hf isotopic compositions and the Nd-Hf model age (T_{DM2}) propose that the Cha Val plutonic rocks were formed by melting of Mesoproterozoic crustal materials with a minor input of mantle-derived components.

Emplacement age of the Cha Val plutonic rocks determined by LA-ICP-MS U-Pb zircon method yielded a narrow age range of 258-249 Ma, corresponding to the Late Permian-Early Triassic. The Cha Val plutonic rocks can be presumably correlated with subduction of the Paleo-Tethys ocean beneath the Indochina block during the Late Permian-Early Triassic.

Acknowledgments

This research was funded by Vietnam National University Ho Chi Minh City (VNU-HCM) under grant number C2020-18-15. We are sincerely thankful to Prof. Tomoyuki Shibata and Prof. Yasutaka Hayasaka of Hiroshima University for their support during the LA-ICP-MS zircon U-Pb dating. We are grateful to Prof. Michel Faure and an anonymous reviewer for their thoughtful and constructive comments and suggestions that helped in improving the presentation and interpretations significantly.

References

Anczkiewicz R., Thirlwall M., Alard O., Rogers N.W., Clark C., 2012. Diffusional homogenization of light REE in garnet from the Day Nui Con Voi Massif in N-Vietnam: Implications for Sm-Nd geochronology and timing of metamorphism in the Red River shear zone. Chemical Geology, 318-319, 16-30.

Barbarin B., 1999. A review of the relationships between granitoid types, their origins and their geodynamic environments. Lithos, 46, 605-626.

Blichert-Toft J., Albarède F., 1997. The Lu-Hf isotope geochemistry of chondrites and the evolution of the mantle-crust system. Earth Planetary Science Letters, 148, 243-258.

Carter A., Roques D., Bristow C., Kinny P., 2001. Understanding Mesozoic accretion in Southeast Asia: Significance of Triassic thermotectonism (Indosinian orogeny) in Vietnam. Geology, 29, 211-214.

Chappell B., 1999. Aluminium saturation in I-and S-type granites and the characterization of fractionated haplogranites. Lithos, 46, 535-551.

Chappell B., White A., 1974. Two contrasting granite types. Pacific Geology, 8, 173-174.

Chen F., Hegner E., Todt W., 2000. Zircon ages and Nd isotopic and chemical compositions of orthogneisses from the Black Forest, Germany: evidence for a Cambrian magmatic arc. International Journal of Earth Sciences, 88, 791-802.

Chen F., Li X.-H., Wang X.-L., Li Q.-L., Siebel W., 2007. Zircon age and Nd-Hf isotopic composition of the Yunnan Tethyan belt, southwestern China. International Journal of Earth Sciences, 96, 1179-1194.

Chu N.-C., Taylor R.N., Chavagnac V., Nesbitt R.W., Boella R.M., Milton J.A., German C.R., Bayon G., Burton K., 2002. Hf isotope ratio analysis using multi-collector inductively coupled plasma mass spectrometry: an evaluation of isobaric interference corrections. Journal of Analytical Atomic Spectrometry, 17, 1567-1574.

Dunkl I., Mikes T., Simon K., Von Eynatten H., 2008. Brief introduction to the Windows program Pepita: data visualization, and reduction, outlier rejection, calculation of trace element ratios and concentrations from LAICPMS data. Mineralogical Association of Canada, Short Course, 40, 334-340.

Faure M., Lepvrier C., Nguyen V.V., Vu T.V., Lin W., Chen Z., 2014. The South China block-Indochina collision: Where, when, and how? Journal of Asian Earth Sciences, 79, 260-274.

Faure M., Nguyen V.V., Hoai L.T.T., Lepvrier C., 2018. Early Paleozoic or Early-Middle Triassic collision between the South China and Indochina Blocks: The controversy resolved? Structural insights from the Kon Tum massif (Central Vietnam). Journal of Asian Earth Sciences, 166, 162-180.

Frost C., Bell J., Frost B., Chamberlain K., 2001. Crustal growth by magmatic underplating: isotopic evidence from the northern Sherman batholith. Geology, 29, 515-518.

Griffin W., Wang X., Jackson S., Pearson N., O'Reilly S.Y., Xu X., Zhou X., 2002. Zircon chemistry and magma mixing, SE China: in-situ analysis of Hf isotopes, Tonglu and Pingtan igneous complexes. Lithos, 61, 237-269.

Harris N.B., Pearce J.A., Tindle A.G., 1986. Geochemical characteristics of collision-zone magmatism. Geological Society, London, Special Publications, 19, 67-81.

Healy B., Collins W., Richards S., 2004. A hybrid origin for Lachlan S-type granites: the Murrumbidgee Batholith example. Lithos, 78, 197-216.

Herzig C.T., Kimbrough D.L., Hayasaka Y., 1997. Early Permian zircon uranium-lead ages for plagiogranites in the Yakuno ophiolite, Asago district, Southwest Japan. Island Arc, 6, 396-403.

Hieu P.T., Anh N.T.Q., Minh P., Thuy N.T.B., 2019. Geochemistry, zircon U-PB ages and HF isotopes of the Muong Luan granitoid pluton, Northwest Vietnam and its petrogenetic significance. Island Arc, 29.

Hieu P.T., Chen F.-k., Thuy N.T.B., Cuong N.Q., Li S.-q., 2013. Geochemistry and zircon U–Pb ages and Hf isotopic composition of Permian alkali granitoids of the Phan Si Pan zone in northwestern Vietnam. Journal of Geodynamics, 69, 106-121.

Hieu P.T., Li S.-Q., Yu Y., Thanh N.X., Dung L.T., Tu V.L., Siebel W., Chen F., 2017. Stages of late Paleozoic to early Mesozoic magmatism in the Song Ma belt, NW Vietnam: evidence from zircon U-Pb

geochronology and Hf isotope composition. International Journal of Earth Sciences, 106, 855-874.

Hieu P.T., Yang Y.-Z., Binh D.Q., Nguyen T.B.T., Dung L.T., Chen F., 2015. Late Permian to Early Triassic crustal evolution of the Kontum massif, central Vietnam: zircon U-Pb ages and geochemical and Nd-Hf isotopic composition of the Hai Van granitoid complex. International Geology Review, 57, 1877-1888.

Hoa T.T., Anh T.T., Phuong N.T., Dung P.T., Anh T.V., Izokh A.E., Borisenko A.S., Lan C.Y., Chung S.L., Lo C.H., 2008. Permo-Triassic intermediate-felsic magmatism of the Truong Son belt, eastern margin of Indochina. Comptes Rendus Geoscience, 340, 112-126.

Hoskin P.W., Schaltegger U., 2003. The composition of zircon and igneous and metamorphic petrogenesis. Reviews in Mineralogy and Geochemistry, 53, 27-62.

Kawaguchi K., Hayasaka Y., Shibata T., Komatsu M., Kimura K., Das K., 2020. Discovery of Paleozoic rocks at northern margin of Sambagawa terrane, eastern Kyushu, Japan: Petrogenesis, U-Pb geochronology and its tectonic implication. Geoscience Frontiers, 11, 1441-1459.

Kawaguchi K., Minh P., Hieu P.T., Cuong T.C., Das K., 2021. Evolution of supracrustal rocks of the Indochina Block: Evidence from new detrital zircon U-Pb ages of the Kontum Massif, Central Vietnam. Journal of Mineralogical and Petrological Sciences, 116, 69-82.

Lan C.-Y., Chung S.-L., Van Long T., Lo C.-H., Lee T.-Y., Mertzman, S. A., Jiun-San Shen, J., 2003. Geochemical and Sr-Nd isotopic constraints from the Kontum massif, central Vietnam on the crustal evolution of the Indochina block. Precambrian Research, 122, 7-27.

Lepvrier C., Maluski H., Van Tich V., Leyreloup A., Truong Thi P., Van Vuong N., 2004. The Early Triassic Indosinian orogeny in Vietnam (Truong Son Belt and Kontum Massif); implications for the geodynamic evolution of Indochina. Tectonophysics, 393, 87-118.

Lepvrier C., Maluski H., Van Vuong N., Roques D., Axente V., Rangin C., 1997. Indosinian NW-trending shear zones within the Truong Son belt (Vietnam) 40Ar-39Ar Triassic ages and Cretaceous to Cenozoic overprints. Tectonophysics, 283, 105-127.

Lepvrier C., Van Vuong N., Maluski H., Truong Thi P., Van Vu T., 2008. Indosinian tectonics in Vietnam. Comptes Rendus Geoscience, 340, 94-111.

Liu J., Tran M.-D., Tang Y., Nguyen Q.-L., Tran T.-H., Wu W., Chen J., Zhang Z., Zhao Z., 2012. Permo-Triassic granitoids in the northern part of the Truong Son belt, NW Vietnam: Geochronology, geochemistry and tectonic implications. Gondwana Research, 22, 628-644.

Ludwig K., 2003. User's manual for isoplot 3.00, a geochronlogical toolkit for microsoft excel. Berkeley Geochronology Center, Special Publication, 4, 25-32.

Maniar P.D., Piccoli P.M., 1989. Tectonic discrimination of granitoids. Geological society of America bulletin, 101, 635-643.

Metcalfe I., 1999. Gondwana dispersion and Asian accretion: an overview. Gondwana dispersion Asian accretion, 9-28.

Metcalfe I., 2013. Gondwana dispersion and Asian accretion: Tectonic and palaeogeographic evolution of eastern Tethys. Journal of Asian Earth Sciences, 66, 1-33.

Middlemost E.A., 1994. Naming materials in the magma/igneous rock system. Earth-Science Reviews, 37, 215-224.

Minh P., Hieu P.T., Hoang N.K., 2018. Geochemical and geochronological studies of the Muong Hum alkaline granitic pluton from the Phan Si Pan Zone, northwest Vietnam: Implications for petrogenesis and tectonic setting. Island Arc, 27.

Nakano N., Osanai Y., Owada M., Binh P., Hokada T., Kaiden H., Bui V.T., 2021. Evolution of the Indochina Block from its formation to amalgamation with Asia: Constraints from protoliths in the Kontum Massif, Vietnam. Gondwana Research, 90, 47-62.

Nakano N., Osanai Y., Owada M., Nam T.N., Charusiri P., Khamphavong K., 2013. Tectonic evolution of high-grade metamorphic terranes in central Vietnam: constraints from large-scale monazite geochronology. Journal of Asian Earth Sciences, 73, 520-539.

Ngo T.X., Santosh M., Tran H.T., Pham H.T., 2016. Subduction initiation of Indochina and South China blocks: insight from the forearc ophiolitic peridotites of the Song Ma Suture Zone in Vietnam. Geological Journal, 51, 421-442.

Nguyen Q.M., Feng Q., Zi J.-W., Zhao T., Tran H.T., Ngo T.X., Tran D.M., Nguyen H.Q., 2019. Cambrian intra-oceanic arc trondhjemite and tonalite in the Tam Ky-Phuoc Son Suture Zone, central Vietnam: Implications for the early Paleozoic assembly of the Indochina Block. Gondwana Research, 70, 151-170.

Osanai, Y., Nakano, N., Owada, M., Nam, T. N., Miyamoto, T., Minh, N. T., Nam, N. V., Tri, T. V., 2008. Collision zone metamorphism in Vietnam and adjacent South-eastern Asia: Proposition for Trans Vietnam Orogenic Belt. Journal of Mineralogical and Petrological Sciences, 103, 226-241.

Owada M., Osanai Y., Nakano N., Matsushita T., Tran Ngoc N., Tsunogae T., Toyoshima T., Binh P., Kagami H., 2007. Crustal anatexis and formation of two types of granitic magmas in the Kontum massif, central Vietnam: Implications for magma processes in collision zones. Gondwana Research, 12, 428-437.

Pearce J.A., Harris N.B., Tindle A.G., 1984. Trace element discrimination diagrams for the tectonic interpretation of granitic rocks. Journal of petrology, 25, 956-983.

Peccerillo A., Taylor S., 1976. Geochemistry of eocene calc-alkaline volcanic rocks from the Kastamonu area, Northern Turkey. Contributions to Mineralogy and Petrology, 58, 63-81.

Peng P., Guo J., Windley B., Liu F., Chu Z., Zhai M., 2012. Petrogenesis of Late Paleoproterozoic Liangcheng charnockites and S-type granites in the central-northern margin of the North China Craton: implications for ridge subduction. Precambrian Research, 222, 107-123.

Qian X., Wang Y., Zhang Y., Zhang Y., Senebouttalath V., Zhang A., He H., 2019. Petrogenesis of Permian-Triassic felsic igneous rocks along the Truong Son zone in northern Laos and their Paleotethyan assembly. Lithos, 328-329, 101-114.

Roger F., Jolivet M., Maluski H., Respaut J.-P., Münch P., Paquette J.-L., Vu Van T., Nguyen Van V., 2014. Emplacement and cooling of the Dien Bien Phu granitic complex: Implications for the tectonic evolution of the Dien Bien Phu Fault (Truong Son Belt, NW Vietnam). Gondwana Research, 26, 785-801.

Sang D.Q., 2011. Petrographic characteristics and zircon U-Pb geochronology of granitoid rocks in the southern Ben Giang, Quang Nam province. Science & Technology Development, 14, 17-30.

Scherer E., Münker C., Mezger K., 2001. Calibration of the lutetium-hafnium clock. Science, 293, 683-687.

Shellnutt J.G., Lan C.-Y., Van Long T., Usuki T., Yang H.-J., Mertzman S.A., Iizuka Y., Chung S.-L., Wang K.-L., Hsu W.-Y., 2013. Formation of Cretaceous Cordilleran and post-orogenic granites and their microgranular enclaves from the Dalat zone, southern Vietnam: Tectonic implications for the evolution of Southeast Asia. Lithos, 182-183, 229-241.

Shi M.-F., Lin F.-C., Fan W.-Y., Deng Q., Cong F., Tran M.-D., Zhu H.-P., Wang H., 2015. Zircon U-Pb ages and geochemistry of granitoids in the Truong Son terrane, Vietnam: Tectonic and metallogenic implications. Journal of Asian Earth Sciences, 101, 101-120.

Sun S.S., McDonough W.F., 1989. Chemical and isotopic systematics of oceanic basalts: implications for mantle composition and processes. Geological Society, London, Special Publications, 42, 313-345.

Thanh N.X., Tu M.T., Itaya T., Kwon S., 2011. Chromian-spinel compositions from the Bo Xinh ultramafics, Northern Vietnam: Implications on tectonic evolution of the Indochina block. Journal of Asian Earth Sciences, 42, 258-267.

Thanh T.V., Hieu P.T., Minh P., Nhuan D.V., Thuy N.T.B., 2019. Late Permian-Triassic granitic rocks of Vietnam: the Muong Lat example. International Geology Review, 61, 1823-1841.

Thuc D.D., Trung H., 1995. Vietnam geology, part of II: magma, Hanoi, Department of Geology and Mineral Resources Survey, Science and Technics Publishing House, 359pp.

Tran H.T., Zaw K., Halpin J.A., Manaka T., Meffre S., Lai C.-K., Lee Y., Le H. V., Dinh S., 2014. The Tam Ky-Phuoc Son Shear Zone in central Vietnam: Tectonic and metallogenic implications. Gondwana Research, 26, 144-164.

Tran T.-H., Polyakov G.V., Tran T.-A., Borisenko A.S., Izokh A.E., Balykin P.A., Ngo T.-P., Pham T.-D., 2016. Permian - Triassic Metallogeny, Intraplate Magmatism and Metallogeny of North Vietnam, 209-252.

Tran T.H., Lan C.-Y., Usuki T., Shellnutt J.G., Pham T.D., Tran T.A., Pham N.C., Ngo T.P., Izokh A.E., Borisenko A.S., 2015. Petrogenesis of Late Permian silicic rocks of Tu Le basin and Phan Si Pan uplift (NW Vietnam) and their association with the Emeishan large igneous province. Journal of Asian Earth Sciences, 109, 1-19.

Tran T.V., Faure M., Nguyen V.V., Bui H.H., Fyhn M.B.W., Nguyen T.Q., Lepvrier C., Thomsen T.B., Tani K., Charusiri P., 2020. Neoproterozoic to Early Triassic tectono-stratigraphic evolution of Indochina and adjacent areas: A review with new data. Journal of Asian Earth Sciences, 191.

Trang N.V., 1994. Geological and mineral map of Vietnamat scale 1:200 000 of the Ba Na sheet Geological survey and and mineral of Viet Nam, Hanoi.

Trang N.V., Tue T., Thị P.T., Long P.H., Thuan P.V., Quyen N.V., Thang N.D., Loc N.Q., 1984. Basic features of geological and mineral structures in Hue-Quang Ngai area. Vietnam geological mapping division, 107-137.

Tri T.V., Khuc V., 2011. Geology and earth resources of Vietnam, Ha Noi, Vietnam, Publishing House for Science and Technology, 634pp.

Usuki T., Lan C.-Y., Tran T.H., Pham T. D., Wang K. -L., Shellnutt G.J., Chung S.-L., 2015. Zircon U-Pb ages and Hf isotopic compositions of alkaline silicic magmatic rocks in the Phan Si Pan-Tu Le region, northern Vietnam: Identification of a displaced western extension of the Emeishan Large Igneous Province. Journal of Asian Earth Sciences, 97, 102-124.

Vinh B.T., 2012. Geological and mineral map of Vietnamat scale 1:50 000 of the A Hoi-Phuoc Hao sheet South Vietnam geological mapping division, Vietnam.

Vuong N.V., Hansen B.T., Wemmer K., Lepvrier C., V. Tich V., Trong Thang T., 2013. U/Pb and Sm/Nd dating on ophiolitic rocks of the Song Ma suture zone (northern Vietnam): Evidence for upper paleozoic paleotethyan lithospheric remnants. Journal of Geodynamics, 69, 140-147.

Wang S., Mo Y., Wang C., Ye P., 2016. Paleotethyan evolution of the Indochina Block as deduced from granites in northern Laos. Gondwana Research, 38, 183-196.

Watson E., Harrison T., 1984. Accessory minerals and the geochemical evolution of crustal magmatic systems: a summary and prospectus of experimental approaches. Physics of the Earth Planetary Interiors, 35, 19-30.

Watson E.B., Harrison T.M., 1983. Zircon saturation revisited: temperature and composition effects in a variety of crustal magma types. Earth Planetary Science Letters, 64, 295-304.

Żelaźniewicz A., Hoa T.T., Larionov A.N., 2013. The significance of geological and zircon age data derived from the wall rocks of the Ailao Shan-Red River Shear Zone, NW Vietnam. Journal of Geodynamics, 69, 122-139.

Zhang R.Y., Lo C.H., Chung S.L., Grove M., Omori S., Iizuka Y., Liou J.G., Tri T.V., 2013. Origin and Tectonic Implication of Ophiolite and Eclogite in the Song Ma Suture Zone between the South China and Indochina Blocks. Journal of Metamorphic Geology, 31, 49-62.